

# Fractional Topological Phases, Flat Bands, and Robust Edge States on Finite Cyclic Graphs via Single-Coin Split-Step Quantum Walks

Dinesh Kumar Panda<sup>1,2,\*</sup> and Colin Benjamin<sup>1,2,†</sup>

<sup>1</sup>*School of Physical Sciences, National Institute of Science Education and Research, Bhubaneswar, Jatni 752050, India*

<sup>2</sup>*Homi Bhabha National Institute, Training School Complex, Anushaktinagar, Mumbai 400094, India*

We report the first realization of a fractional topological phase in a fully unitary, noninteracting discrete-time quantum walk implemented on finite cyclic graphs. Using a single-coin split-step cyclic quantum walk (SCSS-CQW), we uncover topological phenomena that are inaccessible within conventional cyclic quantum-walk dynamics. The protocol enables controlled engineering of quasienergy spectra, flat bands, and topological phase transitions through the step-dependency parameter and coin-rotation angle. We show that cyclic graphs with even and odd numbers of sites exhibit qualitatively different band structures, while rotational flat bands arise exclusively in  $4n$ -site cycles; a general analytic condition for their emergence is derived. The SCSS-CQW produces fractional winding numbers  $\pm\frac{1}{2}$  (Zak phases  $\pm\frac{\pi}{2}$ ), in sharp contrast with the integer invariants of standard quantum walks. These fractional invariants lead to an unconventional bulk–boundary correspondence and support edge states beyond the usual integer topological classification. In the step-dependent protocol, transitions between distinct fractional winding sectors generate robust edge modes. Numerical simulations show that these states remain stable in the presence of both dynamic and static coin disorder as well as phase-preserving perturbations, while survival-probability analysis demonstrates their long-time persistence. Requiring only a constant number of detectors independent of the evolution time, the proposed scheme offers a minimal-resource and experimentally accessible platform for realizing fractional topology, flat bands, and protected edge states in small-scale synthetic quantum systems.

*Introduction.*—Topological phases, characterized by band invariants, protected edge states, and flat bands, constitute a central theme in condensed matter physics and play an important role in quantum memory and topological quantum computation (TQC) [1–3]. Since the discovery of the integer quantum Hall effect [4, 5], followed by the theoretical [6–8] and experimental [9, 10] realization of topological insulators [10, 11], topology has been understood to arise from gapped band structures, where symmetry-protected edge states emerge at the interfaces between distinct phases through the bulk–boundary correspondence [2, 12, 13]. Band-gap closings may appear in different forms, including linear dispersions (Dirac cones), nonlinear structures (Fermi arcs), or dispersionless modes (flat bands). In particular, gapped flat bands can host strong correlation effects such as Mott phases and fractional quantum Hall states, while gapless flat bands are associated with quantum criticality and unconventional transport phenomena [14–18]. Experimental realizations of topological phases have been demonstrated in platforms such as photonic lattices [19] and ultracold atoms and molecules [20, 21]. Despite their potential for robust quantum information storage and noise-resilient state transfer [22–26], naturally occurring topological materials are relatively rare and often constrained by symmetry requirements [27–31]. This limitation has motivated the exploration of synthetic platforms, including discrete-time quantum walks (QWs). Quantum walks describe the coherent lattice evolution of particles

with internal degrees of freedom, governed by interference and entanglement [2, 32–35]. Implementations in one, two, and three dimensions—particularly photonic realizations—have enabled the simulation of a wide range of topological phenomena [1–3, 12, 13, 36–42], providing tunable control over symmetries and access to regimes that are difficult to realize in conventional condensed-matter systems.

Despite these advances, the realization of fractional topological invariants within finite, fully unitary quantum walk architectures remains largely unexplored. In particular, the simulation of topological phenomena using quantum walks on finite cyclic graphs—cyclic quantum walks (CQWs)—has received little attention, with only two studies reported so far [40, 43]. Due to their finite-dimensional Hilbert space, CQWs are particularly resource-efficient for photonic implementations, requiring only a small number of particle detectors and passive optical components (e.g., waveplates or Jones plates) [40, 44, 45], in contrast to conventional QWs defined on extended 1D–3D lattices. Ref. [43] demonstrated integer winding numbers  $\pm 1$  together with gapped flat bands and topological edge states, whereas Ref. [40] considered only the Zak phase for a Hadamard-coin QW on a six-site cycle. Fractional winding numbers  $\pm\frac{1}{2}$  (corresponding to Zak phases  $\pm\frac{\pi}{2}$ ), previously reported mainly in interacting many-body systems [46] or in non-Hermitian settings [47–49], encode exotic phase transitions and unconventional edge states beyond those associated with integer topological invariants [47–49]. These features indicate richer band topology and anomalous bulk–boundary correspondence [47–49]. Notably, the fractional invariants in Refs. [47–49] arise through non-

\* dineshkumar.quantum@gmail.com

† colin.nano@gmail.com

Hermitian mechanisms. In contrast, here we generate fractional winding numbers within a fully unitary framework governed by a Hermitian Hamiltonian in finite, non-interacting systems (small cyclic graphs). Moreover, the emergence of topological flat bands and fractional winding numbers in cyclic graphs, as well as the possibility of engineering robust edge states from them, has not been previously investigated. In this work we address this gap by analyzing the effects of dynamic and static disorder, as well as phase-preserving perturbations, modeling the decay of survival probabilities, and demonstrating the long-time stability of the resulting edge states. Our protocol further requires only a constant number of particle detectors, independent of the evolution time.

*Single coin split-step CQW protocol.*— A CQW describes the evolution of the spatial distribution of a single quantum particle (e.g., an ion, photon, or electron) on a benzene-like ring, i.e., an  $N$ -cycle graph ( $N$  being the number of sites) [40, 43]. The walker evolves in the composite Hilbert space  $\mathcal{H} = \mathcal{H}_P \otimes \mathcal{H}_C$ , consisting of an  $N$ -dimensional position space  $\mathcal{H}_P$  (with basis  $\{|x\rangle \mid x \in \{0\} \cup \mathbb{N}\}$ ) and a two-dimensional coin space  $\mathcal{H}_C$  (with basis  $\{|1_c\rangle, |0_c\rangle\}$ ). Due to the spatial symmetry of the cyclic graph, the CQW dynamics can be diagonalized using the discrete quantum Fourier transform (QFT),

$$|k'\rangle = \frac{1}{\sqrt{N}} \sum_{x=0}^{N-1} e^{i\frac{2\pi}{N}xk'} |x\rangle,$$

where  $k', x \in \{0, 1, 2, \dots, N-1\}$ . At each time step, the particle may move anticlockwise or clockwise depending on the coin state  $|1_c\rangle$  or  $|0_c\rangle$ . This motion is governed by the shift (translation) operator  $\hat{S}$ , conditioned on the action of a single-qubit coin (gate)  $\hat{C}$ . The time-evolution operator of a standard CQW is given by

$$\hat{U}_{\text{evo}} = \hat{S} [I_N \otimes \hat{C}],$$

and the quantum state after  $t$  steps evolves as  $|\psi(t)\rangle = \hat{U}_{\text{evo}}^t |\psi(0)\rangle$ , starting from the initial state  $|\psi(0)\rangle$ . By appropriately modifying the shift and coin operations, the CQW dynamics can be extended to a richer protocol known as the single-coin split-step CQW (SCSS-CQW), which enables distinct topological phenomena that are inaccessible within the standard CQW framework [43]. The topological invariant [40, 43, 50, 51] characterizing the topological phases of our protocol is the winding number [43], i.e.,

$$\omega = \frac{1}{2\pi} \sum_{k'=0}^{N-1} (\vec{n} \times \frac{\partial \vec{n}}{\partial k'}) \cdot \hat{A}. \quad (1)$$

which is obtained via the stroboscopic evolution,  $\hat{U}_{\text{evo}} = e^{-i(\hat{H})}$ ,  $\hat{H} = \vec{\sigma} \cdot \hat{n} * E(k)$ , which by definition is Hermitian, where,  $\hat{A}$  is a vector of unit magnitude (in a quantum Bloch-sphere), and it is orthogonal to the winding vector  $\vec{n}$  for all  $k \in [0, 2\pi]$  (complete Brillouin zone) and  $k = \frac{2\pi k'}{N}$ . A phase is topological if  $w \neq 0$  and trivial if  $w = 0$ .

The temporal evolution of a quantum walker particle evolving via SCSS-CQW dynamics with a single coin  $\hat{C}_\gamma$ , is governed by the operator,  $\hat{U}_{\text{evo}} = \hat{S}_+ \hat{C}_\gamma \hat{S}_- \hat{C}_\gamma$ , where the shift operators are:  $\hat{S}_+ = \sum_{n=0}^{N-1} |0\rangle_c \langle 0|_c \otimes (|x+1\rangle \langle x| + |1\rangle \langle 1| \otimes |x\rangle \langle x|)$ ,  $\hat{S}_- = \sum_{n=0}^{N-1} |0\rangle_c \langle 0|_c \otimes (|x\rangle \langle x| + |1\rangle \langle 1| \otimes |x-1\rangle \langle x|)$ , and the coin,  $\hat{C}_\gamma = e^{-i\frac{D\gamma}{2}\sigma_y}$ .  $\gamma \in [0, 2\pi]$  is the rotation-angle and the step-dependency parameter  $D$  is an integer, i.e.,  $D \geq 2$  refers to a step-dependent (SD) coin while  $D = 1$  refers to a step-independent (SI) coin. In the SCSS-CQW evolution,  $D$  denotes the number of times the single coin is acted at each time-step. In momentum space,  $\hat{S}_+ = e^{-i(\frac{2\pi k}{2N})(\sigma_z + 1)}$ ,  $\hat{S}_- = e^{-i(\frac{2\pi k}{2N})(\sigma_z - 1)}$ . Under stroboscopic evolution  $\hat{U}_{\text{evo}} = e^{-i(\hat{H})}$ , see for more details Supplementary Material (SM) [52] Sec. I, we calculate the energy dispersion in SCSS-CQW as,

$$E_\pm = \pm \cos^{-1} \left[ \cos k (\cos \frac{D\gamma}{2})^2 - (\sin \frac{D\gamma}{2})^2 \right], \quad (2)$$

and winding number (Eq. (1)) for a  $N$ -cycle graph is,

$$\omega_{\gamma, D, N} = \sum_{k'=0}^{N-1} \frac{2 \sin(\frac{2\pi k'}{2N})}{N(2 \cos^2(\frac{k'}{2}) \cos(\gamma D) + \cos(k) - 3)}, \quad \text{with } k = \frac{2\pi k'}{N}. \quad (3)$$

When  $D = 1$ , i.e., SI-SCSS-CQW, and for  $\gamma =$

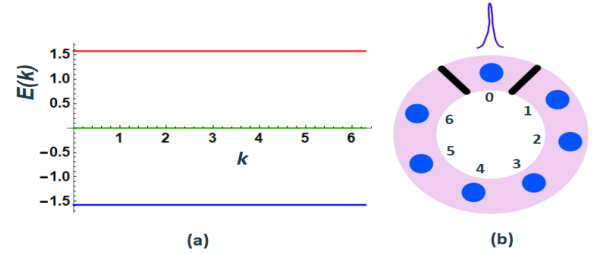


Figure 1. Schematics for (a) symmetric gapped flat-bands (red, blue) and gapless flat-bands (green); (b) creating a phase boundary between site 0 and the remaining sites in a 7-site cycle, where an edge-state (blue peak, which is robust and remains nearly unchanged over time), is expected to appear via SCSS-CQW dynamics. Note: The single-step evolution operator of SCSS-CQW is a composite sequence,  $\hat{U}_{\text{evo}} = \hat{S}_+ \hat{C}_\gamma \hat{S}_- \hat{C}_\gamma$ , involving alternating two conditional shifts and coin rotations, rather than a single homogeneous coin-shift operation,  $\hat{U}_{\text{evo}} = \hat{S} \hat{C}_\gamma$ .

$\frac{\pi}{2}$  and  $N = 3, 4, 7, 8$ , the winding numbers are,  $\omega_{\frac{\pi}{2}, 1, N} = 0.505076, 0.500867, 0.500004, 0.500001$ , which are almost same as with  $N \rightarrow$  very large, i.e.,  $N = 1000$  and  $\omega_{\frac{\pi}{2}, 1, 1000} = \frac{1}{2} = 0.5$ . For  $D = 5$ , i.e., a SD-SCSS-CQW, we obtain,  $\omega_{\frac{\pi}{2}, 5, N} = -0.505076, -0.500867, -0.500004, -0.500001$ , with  $N = 3, 4, 7, 8$ , which is approximately same as for  $N = 1000$ , i.e.,  $\omega_{\frac{\pi}{2}, 5, 1000} = -\frac{1}{2} = -0.5$ . Earlier studies on fractional winding numbers [47–49] involve non-Hermitian Hamiltonians or interacting evolution and 1D infinite lattice, whereas our work is unique in realizing them through a unitary evolution that obeys Hermitian physics with fi-

nite cyclic graphs and operates with minimal resources, see End Matter (EM).

Below, we discuss the generation of topological phases, energy gap closing, flat bands and topological winding numbers, edge states for step-dependent as well as step-independent variants of SCSS-CQW dynamics, on finite even and odd cycle-graphs. We also test robustness of the generated edge states against dynamic-static coin disorder [2, 43, 53, 54] and phase preserving perturbations [2, 43].

*Energy dispersion, topological phases and edge states.*— Quasienergy as a function of momentum  $k$ , and the winding number (topological invariant) as a function of the rotation angle  $\gamma$  [Eqs. (2), (3)], are shown in Fig. 7 for a SI (step-independent) coin ( $D = 1$ ), and in Fig. 3 for a SD (step-dependent) coin ( $D = 2$ ). The case  $D = 3$  is presented in the SM, Sec. I, for  $N = 7, 8$  cycles. Both the SD and SI SCSS-CQW exhibit conducting (energy gap closing) and insulating phases.

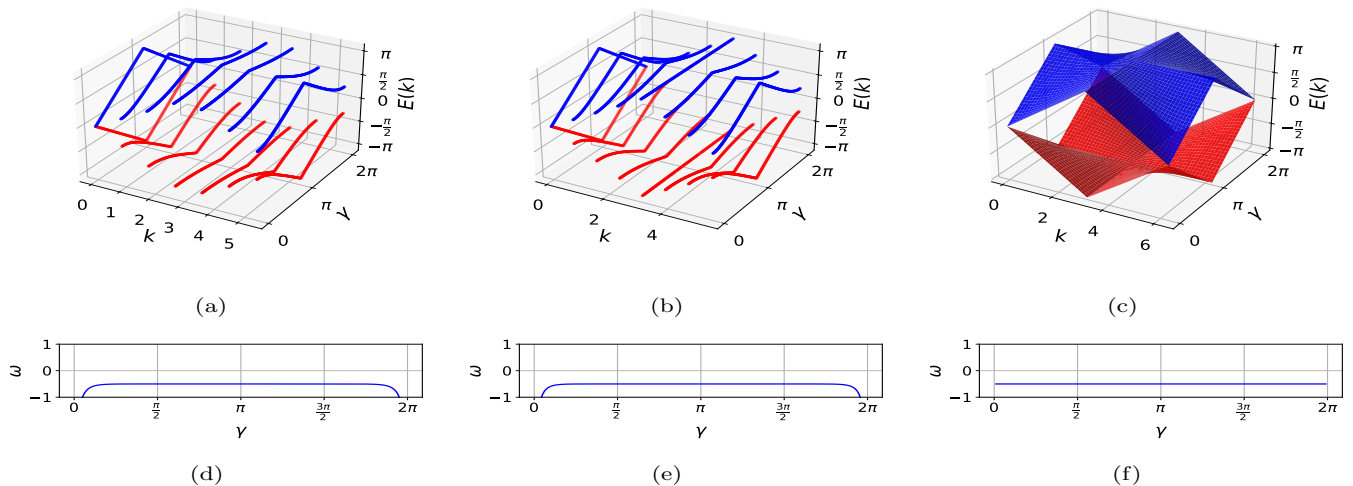


Figure 2. Dependence of quasienergy  $E(k)$  on momentum  $k$  and coin angle ( $\gamma$ ) for: (a) 7-cycle; (b) 8-cycle; (c) 1000-cycle. The red (blue) curves represent the upper (lower) quasienergy branches. (d)–(f) The corresponding winding number  $\omega$  as a function of  $\gamma$  for the 7-cycle, 8-cycle, and 1000-cycle, respectively, obtained using the SI SCSS-CQW protocol with  $D = 1$ . A fractional winding number of  $-\frac{1}{2}$  is observed, with no phase transition.

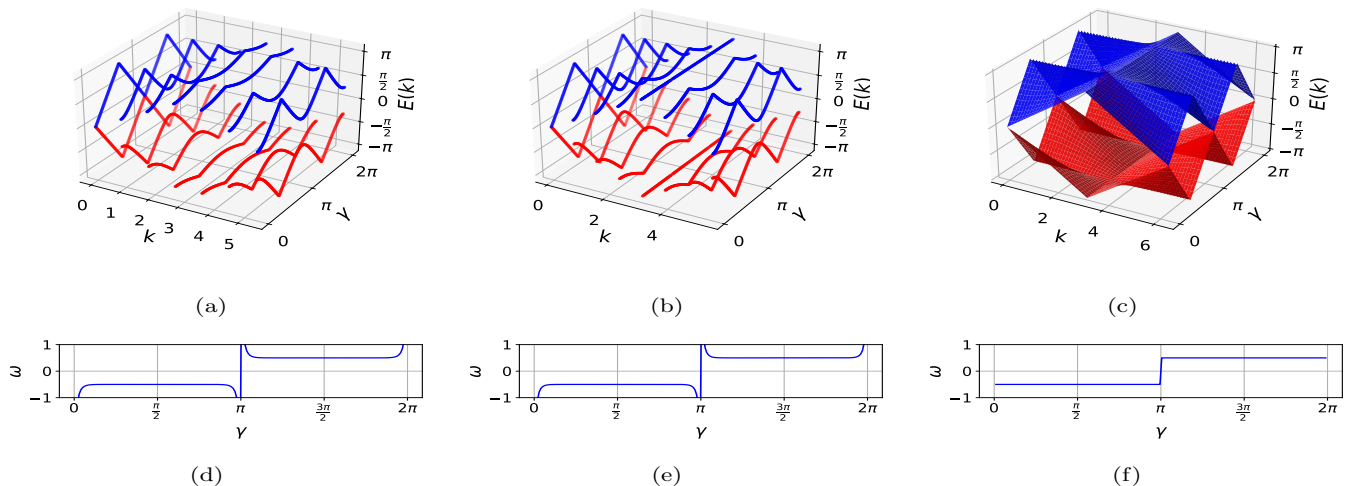


Figure 3. Dependence of quasienergy  $E(k)$  on momentum  $k$  and coin angle ( $\gamma$ ) for: (a) 7-cycle; (b) 8-cycle; (c) 1000-cycle. The red (blue) curves represent the upper (lower) quasienergy branches. (d)–(f) The corresponding winding number  $\omega$  as a function of  $\gamma$  for the 7-cycle, 8-cycle, and 1000-cycle, respectively, obtained using the SD SCSS-CQW protocol with  $D = 2$ . Fractional winding numbers  $\pm\frac{1}{2}$  are observed, with a phase transition occurring at  $\gamma = \pi$ .

The phases are purely topological with a fractional winding number  $w = -\frac{1}{2}$  in SI-SCSS-CQW. In contrast, SD-SCSS-CQW ( $D \geq 2$ ) supports two distinct topological phases ( $w = \pm\frac{1}{2}$ ) and exhibits topological phase transitions that can be induced by tuning the rotation angle  $\gamma$ . The number of topological phase transitions increases linearly with  $D$ ; for instance, a single phase transition occurs for  $D = 2$ , two transitions for  $D = 3$ , and three for  $D = 4$ . The number of gapped flat bands (GFBs), characterized by zero group velocity, follows a similar trend: one GFB for  $D = 1$ , two GFBs for  $D = 2$ , and so on.

In SM Sec. I, we analytically derive the condition for obtaining GFBs in our protocol, given by  $\gamma = \frac{(2n+1)\pi}{D}$ , where  $n \in \mathbb{Z}_+ \cup \{0\}$ . A notable feature of the topological phases in SCSS-CQW evolution is the emergence of topological edge states, which can appear at the boundary (interface) between two different phases in a cyclic graph, see Fig. 1(b). The presence of phase transitions in SD-SCSS-CQW enables the occurrence of such topological edge states for  $D \geq 2$ , which is not possible in the  $D = 1$  case.

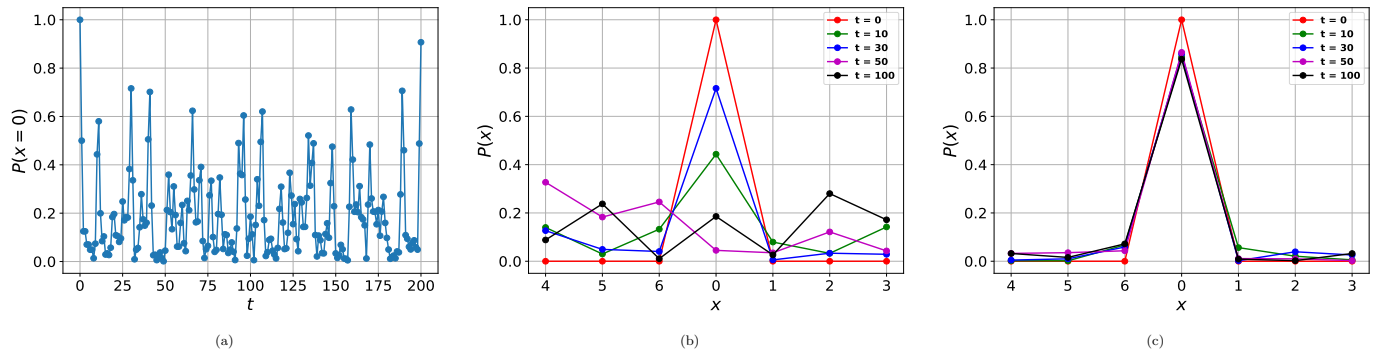


Figure 4. (a) Spatial probability  $P(0)$  of the walker at site 0 as a function of discrete time steps  $t$  for rotation angle  $\gamma = \frac{3\pi}{4}$ . (b) A uniform topological phase ( $\omega = -\frac{1}{2}$  for  $\gamma = \frac{3\pi}{4}$ ) produces no boundary and therefore no edge state, as reflected in the probability profile  $P(x)$  versus  $x$  at different  $t$ . (c) Introducing an interface between two distinct topological phases ( $\omega = \frac{1}{2}$  for  $\gamma = \frac{6\pi}{4}$  and  $\omega = -\frac{1}{2}$  for  $\gamma = \frac{3\pi}{4}$ ) results in a robust edge state localized at site  $x = 0$ , persisting over time, as demonstrated using the SD SCSS-CQW protocol ( $D = 2$ ) on a 7-site cyclic graph.

In Fig. 4, the walker is initialized in the state

$$|\psi(0)\rangle = |0\rangle \otimes \frac{1}{\sqrt{2}} (|1_c\rangle + |0_c\rangle),$$

on a seven-site cyclic graph. The coin operator at position 0 is chosen with parameter  $\gamma = \frac{6\pi}{4}$  (corresponding to  $\omega = \frac{1}{2}$ ), whereas at all other sites the coin parameter is fixed to  $\gamma = \frac{3\pi}{4}$  (i.e.,  $\omega = -\frac{1}{2}$ ). This spatial modulation of the coin parameter induces a topological phase boundary localized at site 0. A pronounced probability amplitude at site 0 serves as a hallmark of an edge state [2, 31, 42, 43] and we observe resilient edge-states, which are stable over a long time ( $t$ ), see Fig. 4(c). The algorithm used to generate the edge state is given in SM Sec. III and the Python code is available in GitHub [55]. We model the possible decay of survival probabilities of the edge state vs time  $t$ , in Fig. 12, and it follows a constant fit (saturation around 0.85), i.e., no decay. In comparison, the edge state generated via SS-QW's on 1D lattice shows a rapidly decaying power law fit [36, 42]. This shows that the generated edge states of this letter remain stable for a very long time, see SM Sec. II for more details.

Our numerical simulations demonstrate that the edge states generated on finite cyclic graphs using the SCSS-CQW protocol remain stable under both moderate dynamic-static gate disorder and phase-preserving perturbations that conserve the winding number; see SM Sec. I.D. This resilience to noise and disorder underscores the strong potential of these edge states for fault-tolerant quantum information processing and topological quantum computing applications.

**Photonic realization.**—Our SCSS-CQW protocol can be experimentally implemented using single photons, which effectively simulate cyclic quantum walkers, together with passive optical components such as waveplates, Jones plates, and polarizing beam splitters (PBS) to realize the shift and coin (gate) operations [2, 40, 44]. The coin degree of freedom is encoded in the polarization of the photon, while the position space can be represented either by spatial modes or by the orbital angular momentum (OAM) of photons [2, 40, 44].

A sequence of PBS and Jones plates can implement the shift operators required in the SCSS-CQW protocol, while the site-dependent rotation angles defining the interface between different topological phases can be locally

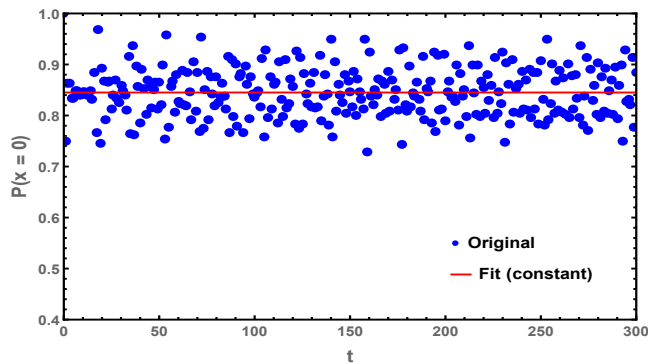


Figure 5. Edge-state survival probability  $P(x = 0)$  vs time step  $t$  using SD SCSS-CQW ( $D = 2$ ) on a 7-cycle graph, without any disorder. The numerical data exhibit fluctuations around a constant mean value 0.85, and are well captured by a constant fit (red), demonstrating long-time saturation and the stability of the localized edge state.

controlled by appropriately adjusting the orientation of the waveplates or Jones plates. The resulting probability distribution can be detected using single-photon detectors; in particular, a pronounced peak at the boundary site provides a clear experimental signature of the edge states generated by our protocol.

*Summary.*— We introduced a new quantum walk protocol, the SCSS-CQW on small finite cyclic graphs, which generates exotic topological phases characterized by fractional winding numbers that are inaccessible using standard CQW schemes. Moreover, these topological effects are achieved with significantly reduced resource consumption compared with existing approaches (see EM I). Even and odd cycles exhibit distinct energy dispersions, and rotational flat bands arise exclusively in graphs with  $4n$  sites ( $n = 1, 2, \dots$ ) with step-dependency  $D \geq 1$  in the protocol. We analytically and numerically demonstrate that the protocol generates topological gapped flat bands, and we derive a general condition for the rotation angle ( $\gamma$ ) and  $D$  that yields flat bands (i.e.,

with zero group velocity); see also SM Sec. I.B.

The SCSS-CQW protocol produces fractional winding numbers  $\{\pm\frac{1}{2}\}$ , in contrast to the integer winding numbers  $\{\pm 1\}$  obtained in standard CQW. In addition, we observe topological phase transitions for  $D \geq 2$ , with the number of transitions and flat bands increasing with  $D$ . These topological properties can be precisely controlled through the step-dependency parameter ( $D \geq 1$ ), the system size, and the coin rotation angle. The emergence of distinct winding numbers (i.e., phase transitions) for  $D \geq 2$  enables the creation of a phase boundary in real position space, leading to the formation of topological edge states. Numerical simulations confirm that the generated edge states remain robust against small dynamic and static disorder as well as perturbations that preserve the topological phase (see SM Sec. I.D). We further model the decay of survival probabilities as a function of time, both with and without disorder, and demonstrate the long-time stability of these edge states (see SM Sec. II).

Furthermore, this protocol can be experimentally implemented using single photons as cyclic quantum walkers, where the initial state is encoded in the photon polarization and the position degree of freedom is represented by spatial modes. Optical elements realize the shift and coin operations, while the site-dependent rotation angles defining the topological phase boundaries can be locally tuned using waveplates and Jones plates to generate photonic edge states. These key findings are summarized in EM II. This work provides a versatile and experimentally accessible platform for generating and controlling fractional topological phases with nontrivial phase transitions, flat bands, and robust edge states in miniaturized synthetic quantum systems. Such capabilities open new avenues toward fault-tolerant quantum computing, simulation of nontrivial topological insulators, robust quantum memory, fault-tolerant quantum architectures, quantum state engineering, and topological quantum cryptography.

- 
- [1] K. Wang, et al., Simulating dynamic quantum phase transitions in photonic quantum walks, *Phys. Rev. Lett.* 122 (2019) 020501.
  - [2] L. Xiao, et al., Observation of topological edge states in parity-time-symmetric quantum walks, *Nature Physics* volume 13, pages1117–1123 (2017).
  - [3] F. Cardano, et al., Statistical moments of quantum-walk dynamics reveal topological quantum transitions, *Nat. Commun.* 7 (2016) 11439.
  - [4] D.J.Thouless, M.Kohmoto, M.P.Nightingale, and M. den Nijs, Quantized Hall Conductance in a Two-Dimensional Periodic Potential, *Phys. Rev. Lett.* 49, 405 (1982).
  - [5] K. v. Klitzing, G. Dorda, and M. Pepper, New Method for High-Accuracy Determination of the Fine-Structure Constant Based on Quantized Hall Resistance, *Phys. Rev. Lett.* 45, 494 (1980).
  - [6] C. L. Kane and E. J. Mele,  $Z_2$  Topological Order and the Quantum Spin Hall Effect, *Phys. Rev. Lett.*95, 146802 (2005).
  - [7] B. A. Bernevig, T. L. Hughes, and S.-C. Zhang, Quantum Spin Hall Effect and Topological Phase Transition in HgTe Quantum Wells, *Science* 314, 1757 (2006).
  - [8] L. Fu and C. L. Kane, Topological insulators with inversion symmetry, *Phys.Rev.B* 76, 045302 (2007).
  - [9] M. Koenig, et al., Quantum Spin Hall Insulator State in HgTe Quantum Wells, *Science* 318, 766 (2007).
  - [10] D. Hsieh et al., A topological Dirac insulator in a quantum spin Hall phase, *Nature (London)* 452, 970 (2008).
  - [11] X.-L. Qi, T. L. Hughes, and S.-C. Zhang, Topological field theory of time-reversal invariant insulators, *Phys.*

- Rev. B 78, 195424 (2008).
- [12] S. Panahiyan and S. Fritzsche, Controllable simulation of topological phases and edge states with quantum walk, *Physics Letters A* 384, 126828 (2020).
- [13] S. Panahiyan and S. Fritzsche, Toward simulation of topological phenomena with one-, two-, and three-dimensional quantum walks, *PHYSICAL REVIEW A* 103, 012201 (2021).
- [14] Evelyn Tang, Jia-Wei Mei, and Xiao-Gang Wen, High-Temperature Fractional Quantum Hall States, *Phys. Rev. Lett.* 106, 236802 (2011).
- [15] Wenjuan Zhang, Zachariah Addison, and Nandini Trivedi, Orbital frustration and topological flat bands, *Phys. Rev. B* 104, 235202 (2021).
- [16] Yuan Cao, et al., Correlated insulator behaviour at half-filling in magic-angle graphene superlattices, *Nature* volume 556, pages80–84 (2018).
- [17] Y.-H. Chan, Ching-Kai Chiu, M. Y. Chou, and Andreas P. Schnyder, Ca3P2 and other topological semimetals with line nodes and drumhead surface states, *Phys. Rev. B* 93, 205132, (2016).
- [18] Shunye Gao, et al., Discovery of a Single-Band Mott Insulator in a van der Waals Flat-Band Compound, *Phys. Rev. X* 13, 041049 (2023).
- [19] J. Otterbach, et al., Effective Magnetic Fields for Stationary Light, *Phys. Rev. Lett.* 104, 033903 (2010).
- [20] N. Goldman, et al., Non-Abelian Optical Lattices: Anomalous Quantum Hall Effect and Dirac Fermions, *Phys. Rev. Lett.* 103, 035301 (2009).
- [21] A. Micheli, G. K. Brenner, and P. Zoller, A toolbox for lattice-spin models with polar molecules, *Nat. Phys.* 2, 341 (2006).
- [22] Kamil P. Michnicki, 3D Topological Quantum Memory with a Power-Law Energy Barrier, *Phys. Rev. Lett.* 113, 130501 (2014).
- [23] Sam Roberts and Stephen D. Bartlett, Symmetry-Protected Self-Correcting Quantum Memories, *Phys. Rev. X* 10 031041 (2020).
- [24] Xiaqi Zhou, Weixuan Zhang, Houjun Sun, and Xiangdong Zhang, Observation of flat-band localization and topological edge states induced by effective strong interactions in electrical circuit networks, *Phys. Rev. B* 107, 035152 (2023).
- [25] G. M. A. Almeida et al., Flat-band quantum communication induced by disorder, *Phys. Rev. A* 108, 022407 (2023).
- [26] Jesse J. Slim, Javier del Pino and Ewold Verhagen, Programmable synthetic magnetism and chiral edge states in nano-optomechanical quantum Hall networks, *Nature Communications* 16, 7471 (2025).
- [27] B. I. Halperin, Quantized Hall conductance, current-carrying edge states, and the existence of extended states in a two-dimensional disordered potential, *Phys. Rev. B* 25, 2185 (1982).
- [28] M. Z. Hasan and C. L. Kane, Colloquium: Topological insulators, *Rev. Mod. Phys.* 82, 3045 (2010).
- [29] A. P. Schnyder, S. Ryu, A. Furusaki, and A. W. W. Ludwig, Classification of topological insulators and superconductors in three spatial dimensions, *Phys. Rev. B* 78, 195125 (2008).
- [30] T. Zhang, Y. Jiang, Z. Song, H. Huang, Y. He, Z. Fang, H. Weng, and C. Fang, Catalogue of topological electronic materials, *Nature* 566, 475 (2019).
- [31] C. M. Chandrashekar, H. Obuse, Th. Busch, Entanglement Properties of Localized States in 1D Topological Quantum Walks, arXiv:1502.00436v2 [quant-ph] (2015).
- [32] Y. Aharonov, L. Davidovich, and N. Zagury, Quantum random walks, *Phys. Rev. A* 48, 1687 (1993).
- [33] Ina Heckelmann, et al., Quantum walk comb in a fast gain laser, *Science* 382, 434 (2023).
- [34] Joshua Feis, Sebastian Weidemann, Tom Sheppard, Hannah M. Price and Alexander Szameit, Space-time-topological events in photonic quantum walks, *Nature Photonics* 19, 518 (2025).
- [35] Cinthia Huerta Alderete, et al., Quantum walks and Dirac cellular automata on a programmable trapped-ion quantum computer, *Nature Communications* 11, 3720 (2020).
- [36] Takuya Kitagawa, et al., Observation of topologically protected bound states in photonic quantum walks, *Nat. Commun.* 3, 882 (2012).
- [37] F. Cardano, et al., Detection of Zak phases and topological invariants in a chiral quantum walk of twisted photons, *Nat. Commun.* 8 (2017) 15516.
- [38] L. Xiao, et al., Higher winding number in a nonunitary photonic quantum walk, *Phys. Rev. A* 98 (2018) 063847.
- [39] X. Wang, et al., Detecting topological invariants and revealing topological phase transitions in discrete-time photonic quantum walks, *Phys. Rev. A* 98 (2018) 013835.
- [40] Farshad Nejdassattari, Yingwen Zhang, Frédéric Bouchard, Hugo Larocque, Alicia Sit, Eliahu Cohen, Robert Fickler, and Ebrahim Karimi, Experimental realization of wave-packet dynamics in cyclic quantum walks, Vol. 6, No. 2, *Optica* (2019).
- [41] J. K. Asbóth, Symmetries, topological phases, and bound states in the one-dimensional quantum walk, *Phys. Rev. B* 86, 195414 (2012).
- [42] Takuya Kitagawa, Mark S. Rudner, Erez Berg, and Eugene Demler, Exploring topological phases with quantum walks, *PHYSICAL REVIEW A* 82,033429 (2010).
- [43] Dinesh Kumar Panda and Colin Benjamin, Quantum walks reveal topological flat bands, robust edge states and topological phase transitions in cyclic graphs, arXiv:2507.17250 [quant-ph] (2025).
- [44] Z.-H. Bian, J. Li, X. Zhan, J. Twamley, and P. Xue, Experimental implementation of a quantum walk on a circle with single photons, *Phys. Rev. A* 95, 052338 (2017).
- [45] Dinesh Kumar Panda and Colin Benjamin, Recurrent generation of maximally entangled single-particle states via quantum walks on cyclic graphs, *Phys. Rev. A* 108, L020401 (2023).
- [46] F. Grusdt et al., *Phys. Rev. Lett.* 110, 260405 (2013); L. Fidkowski and A. Kitaev, *Phys. Rev. B* 81, 134509 (2010).
- [47] Yang, M., Liao, et al., Observing half-integer topological winding numbers in non-Hermitian synthetic lattices, *Light: Science & Applications* 14 225 (2025).
- [48] Wengang Zhang, et al., Observation of Non-Hermitian Topology with Nonunitary Dynamics of Solid-State Spins, *Phys. Rev. Lett.* 127, 090501 (2021).
- [49] Xiao-Ran Wang, Cui-Xian Guo, and Su-Peng Kou, Defective edge states and number-anomalous bulk-boundary correspondence in non-Hermitian topological systems, *Phys. Rev. B* 101, 121116(R) (2020).
- [50] Filippo Cardano, et. al, Detection of Zak phases and topological invariants in a chiral quantum walk of twisted photons. *Nature Communications* 8, 15516 (2017).
- [51] S. Panahiyan and S. Fritzsche, Controllable simulation of

- topological phases and edge states with quantum walk, *Physics Letters A* 384 126828 (2020).
- [52] Dinesh Kumar Panda and Colin Benjamin, Supplementary Material for additional details of the Letter which contains the Refs. [2, 17, 18, 31, 40, 42–44, 53, 55–67], [Link to be provided by Publisher team] (2026).
- [53] Dinesh Kumar Panda and Colin Benjamin, Phase vs coin vs position disorder as a probe for the resilience and revival of single particle entanglement in cyclic quantum walks, *Physical Review E* 111, L042103, (Letter) (2025).
- [54] Louie Hong Yao and Sascha Wald, Coined quantum walks on the line: Disorder, entanglement, and localization, *Phys. Rev. E* 108, 024139 (2023).
- [55] Dinesh Kumar Panda and Colin Benjamin, Python code to generate edge states using step-dependent SCSS-CQW dynamics, Link: <https://github.com/Quantum-Panda97/Edge-states-using-step-dependent-SCSS-CQW-dynamics> (2026).
- [56] Robert W. Keyes, Correlation between Mobility and Effective Mass in Semiconductors, *Journal of Applied Physics*, vol. 30, no. 3, pp. 454, (1959).
- [57] Cian C. Reeves, Scott K. Cushing, Vojtech Vlcek, The role of effective mass and long-range interactions in the band-gap renormalization of photo-excited semiconductors, arXiv:2503.09715 [cond-mat.mtrl-sci] (2025).
- [58] Xinyu Chen, Shuaihua Lu, Qian Chen, Qionghua Zhou and Jinlan Wang, From bulk effective mass to 2D carrier mobility accurate prediction via adversarial transfer learning, *Nature Communications* 15, 5391 (2024).
- [59] H. B. Perets *et al.*, Realization of quantum walks with negligible decoherence in waveguide lattices, *Phys. Rev. Lett.* 100, 170506 (2008).
- [60] A. Peruzzo, *et al.*, Quantum walks of correlated photons, *Science* 329, 1500 (2010).
- [61] A. Schreiber, *et al.*, Photons walking the line: A quantum walk with adjustable coin operations, *Phys. Rev. Lett.* 104, 050502 (2010).
- [62] M. A. Broome, *et al.*, Discrete single-photon quantum walks with tunable decoherence, *Phys. Rev. Lett.* 104, 153602 (2010).
- [63] M. Tamura, T. Mukaiyama, and K. Toyoda, Quantum walks of a phonon in trapped ions, *Phys. Rev. Lett.* 124, 200501 (2020).
- [64] H. Schmitz, *et al.*, Quantum walk of a trapped ion in phase space, *Phys. Rev. Lett.* 103, 090504 (2009).
- [65] F. Zähringer, *et al.*, Realization of a quantum walk with one and two trapped ions, *Phys. Rev. Lett.* 104, 100503 (2010).
- [66] C. A. Ryan, M. Laforest, J. C. Boileau, and R. Laflamme, Experimental implementation of a discrete-time quantum random walk on an NMR quantum-information processor, *Phys. Rev. A* 72, 062317 (2005).
- [67] Wei-Wei Zhang, Sandeep K. Goyal, Christoph Simon, and Barry C. Sanders, Decomposition of split-step quantum walks for simulating Majorana modes and edge states, *Phys. Rev. A* 95, 052351 (2017).

## END MATTER

## I. RESOURCE OVERHEAD

The total experimental cost, or resource overhead of the CQW protocol is determined by the number of coin and shift operators required, together with the number of detectors used for readout. In this letter, we quantify this overhead for the SCSS-CQW protocol and compare them with existing split-step (SS-QW) and split-coin (SC-QW) protocols [2, 31, 42, 67] on 1D lattices, which are widely used to generate topological phases, and edge-states in photon-based experiments [2, 44, 67]. The SCSS-CQW protocol substantially lowers the required experimental resources, as these use fewer coin operations and only a small number of single-photon detectors, unlike SS-QW and SC-QW protocols. Specifically, the SCSS-CQW protocol reduces the total resource count by almost a factor of two, with detector requirements scaling far more favorably compared with the  $O(2\tau)$  scaling of existing schemes for a walk of  $\tau$  steps. This significant reduction improves the practicality of implementing the SCSS-CQW protocol for realizing topological phases and edge states across photonic and other quantum platforms [59–66]. A detailed comparison of resource costs is provided in Table I.

Protocol	Distinct coins (# $\theta$ )	Detectors (# $d$ )	Shift operators (# $s$ )	Coin operators (# $c$ )	Resource overhead ( $R = \#_d + \#_s + \#_c + \#_\theta$ )
<b>This letter: SCSS-CQW protocol (for <math>N</math>, e.g., 7, 8,...)</b>					
SCSS-CQW	2	$N$	$2\tau$	$2\tau$	$R_{SCSS} = 4\tau + N + 2$
<b>Example: This letter: SCSS-CQW protocol (<math>N = 8</math>, <math>\tau = 100</math>)</b>					
SCSS-CQW	2	8	200	200	$R_{SCSS} = 410$
<b>QW: Quantum walks on 1D lattices (for <math>N_L</math>, e.g., 100, 200, 1000,...)</b>					
SS-QW	3	$(2\tau + 1)$	$2\tau$	$2\tau$	$R_{SS} = 4\tau + (2\tau + 1) + 3$
SC-QW	3	$(2\tau + 1)$	$2\tau$	$2\tau$	$R_{SC} = 4\tau + (2\tau + 1) + 3$
<b>Example: QW: Quantum walks on 1D lattices (<math>N_L = 100</math>, <math>\tau = 100</math>)</b>					
SS-QW	3	201	200	200	$R_{SS} = 604$
SC-QW	3	201	200	200	$R_{SC} = 604$

TABLE I. Comparison of resource overhead in implementing different quantum walk protocols, i.e., the SCSS-CQW protocol on cyclic graphs vs. existing QW on infinite 1D lattice via SS-QW and SC-QW protocols, to generate topological phases, and protected edge-states. Note: Here  $N_L$  denotes the number of sites on a 1D lattice and  $N$  denotes number of position sites in a cyclic lattice or graph, while  $\tau$  represents the number of time steps in the quantum walk.

The time-evolution of the quantum particle (walker) via our SCSS-CQW is governed by the following evolution operator,  $\hat{U}_{evo,SSCQW} = \hat{S}_+ \hat{C}_\gamma \hat{S}_- \hat{C}_\gamma$ , where the shift operators are:  $\hat{S}_+ = \sum_{n=0}^{N-1} |0\rangle_c \langle 0|_c \otimes (|x+1\rangle \langle x| + |1\rangle \langle 1| \otimes |x\rangle \langle x|)$ ,  $\hat{S}_- = \sum_{n=0}^{N-1} |0\rangle_c \langle 0|_c \otimes (|x\rangle \langle x| + |1\rangle \langle 1| \otimes |x-1\rangle \langle x|)$ , and the coin operator has the form,  $\hat{C}_\gamma = e^{-i\frac{D\tau}{2}\sigma_y}$ .

Similarly, the time-evolution operators of the quantum walker evolving by split-step quantum-walks (SS-QW) and split-coin quantum-walks (SC-QW) on nonperiodic

1D lattices, are given by,

$$\begin{aligned} \text{for SS-QW: } U_{SS} &= \hat{S}_+ \hat{C}_a \hat{S}_- \hat{C}_b \\ \text{and for SC-QW: } U_{SC} &= \hat{S} \hat{C}_a \hat{S} \hat{C}_b, \end{aligned} \quad (4)$$

where the shift operator,  $\hat{S} = e^{-i\frac{2\pi}{N}k'\sigma_z}$ .

If  $|\psi(0)\rangle$  represents walker's initial state, then the quantum mechanical state at the later timestep  $t$  becomes,  $|\psi(t)\rangle = U^t(|\psi(0)\rangle)$ .

The evolution operators of our SCSS-CQW protocol, and existing SS-QW ( $U_{SS}$ ), and SC-QW ( $U_{SC}$ ), at time  $t = \tau$ , have the forms,

$$\begin{aligned} \hat{U}_{evo,SSCQW}^\tau &= (\hat{S}_+ \hat{C}_\gamma \hat{S}_- \hat{C}_\gamma)^\tau, U_{SS}^\tau = (\hat{S}_+ \hat{C}_a \hat{S}_- \hat{C}_b)^\tau, \\ \text{and } U_{SC}^\tau &= (\hat{S}_f \hat{C}_a \hat{S}_f \hat{C}_b)^\tau. \end{aligned} \quad (5)$$

One can explicitly determine the resource overhead, namely the scaling of the total number of operators required and the number of detectors involved. The operators here refer to both coin and shift operators. In our SCSS-CQW protocol, as well as in the existing protocols, each time step consists of four such operators (two coin and two shift operators), as given in Eq. (5). Consequently, after  $\tau$  time steps, the operator count scales as in all mentioned protocols as,  $2\tau + 2\tau = 4\tau$ .

However, our SCSS-CQW protocol offers a dramatic reduction in the number of particle detectors required. In each case, the number of detectors is fixed and equals to the count of lattice sites in the small cyclic (periodic) graph ( $N = 7, 8, \dots$ ), and it does not depend on the number of time steps in the walk. By contrast, both the SS-QW and SC-QW schemes require  $(2\tau + 1)$  detectors for a walk of  $\tau$  steps, leading to a detector overhead that grows linearly with time. Consequently, our protocol exhibits an  $O(1)$  detector scaling in contrast to the  $O(2\tau)$  scaling of the existing 1D quantum walk schemes [2, 31, 42, 67] to generate edge states via integer winding numbers. Thus, our protocol not only generates fractional topological phases it also greatly improves the scalability and practical implementation of topological phase detection and edge-state generation on photonic and other quantum platforms.

Furthermore, the SCSS-CQW protocol needs only two different coin operators (two choices of  $\hat{C}_\gamma$ ) to engineer a phase boundary in real position space, an essential component for producing edge states. In contrast, SS-QW and SC-QW rely on three distinct coins (two versions of  $\hat{C}_b$  and a fixed  $\hat{C}_a$  in SS-QW/SC-QW) to create the same boundary.

Taking all resources into account, the total overhead for our SCSS-CQW protocol is,  $R_{SSCQW} = 4\tau + N + 2$ , as compared to the significantly larger overhead of  $R_{SS}, R_{SC} = 4\tau + (2\tau + 1) + 3$  in the exiting SS-QW or SC-QW protocols, as juxtaposed in the Table I.

Example: Consider a cyclic quantum walk with

$N = 8$  sites and  $\tau = 100$  time steps. Our SCSS-CQW protocol requires a total resource overhead  $R_{\text{SSCQW}} = 4\tau + N + 2 = 410$ . In comparison, the SS-QW or SC-QW protocol demands  $R_{\text{SS}}, R_{\text{SC}} = 4\tau + (2\tau + 1) + 3 = 604$ . This shows that our construction lowers the total experimental resources by more than a factor of **0.32**. In absolute terms, this corresponds to a reduction of 194 components (detectors plus operators), which amounts to a relative saving of approximately **32%**, without compromising the ability to generate topological phase boundaries and edge states. Such a substantial decrease in operational and detection requirements highlights the enhanced experimental efficiency and practical implementability of the SCSS-CQW protocol.

## II. ANALYSIS

Analytical calculations (Eqs. 2-3 of the letter and Eqs. 7-9, 12, 15 of SM) and numerical simulations (Figs. 2-5 of the letter and Figs. 1-3 of SM) show that SD ( $D \geq 2$ ), and SI ( $D = 1$ ) SCSS-CQW on finite cycle graphs show topological effects. We see topological phases (with fractional winding-numbers), rotational flatbands for  $4n$ -site cycle graphs ( $n$  is a positive integer), for  $D \geq 2$  and topological flatbands, along with resilient edge states generation. We explicitly show that the resulting topological edge states remain robust against weak and intermediate disorder (see SM Sec. I.D). Table II juxtaposes our key findings on the SD and SI versions of SCSS-CQW on even and odd cycles, which are discussed below.

The SI version of SCSS-CQW shows energy band closing in even and odd cycles. Gap closing occurs in SD versions of SCSS-CQW, too. Even cycles show more number of gap closing points compared to odd cycles. Rotational flat-bands appear for the case of  $4n$ -cycles (where,  $n \in \mathbf{N}$ ) for  $D \geq 2$  onward in SD version of SCSS-CQW. This implies that the energy bands of the SCSS-CQW evolution become independent of the quantum coins. The SD version of SCSS-CQW shows topological gapped flat-bands (topological) and are linked to studies on quantum criticality and exotic transport in semimetals [17, 18].

The SI version of SCSS-CQW does not show a phase transition, i.e., a constant winding number ( $-\frac{1}{2}$ ) throughout rotation space. In addition, the SD-SCSS-CQW generates two fractional winding numbers:  $\pm\frac{1}{2}$ . Furthermore, the presence of phase transition in SD version of SCSS-CQW makes it suitable to realize edge states by creating phase boundary in real space for  $D \geq 2$ . We have also demonstrated the generation of edge states via SCSS-CQW, see Figs. 4.

From numerical simulations (Figs. 4-13 of SM), we show that the topologically protected edge states generated via the SCSS-CQW protocol are robust against

Model	Feature	Odd (7) Cycle	Even (8) Cycle
SI-SCSS-CQW ( $D = 1$ )	Band closing	Yes, at $k = 0$ but not at $k \neq 0$ .	Yes, at both $k = 0$ and $k \neq 0$ and for more $k \neq 0$ values than odd cycles.
	Flatband	Yes and gapped with $k, \&$ for a single coin.	Yes and gapped in $k, \&$ for a single coin.
	Rotational flatband	Not possible.	Yes.
	Topological winding number	Fractional & topological ( $\omega = \frac{1}{2}$ )(One value, No phase transition).	Fractional & topological ( $\omega = \frac{1}{2}$ )(One value, No phase transition).
	Edge states	Not possible.	Not possible.
SD-SCSS-CQW ( $D \geq 2$ )	Band closing	Yes, at $k = 0$ , but not at $k \neq 0$ .	Yes, at both $k = 0$ and $k \neq 0$ and for more $k \neq 0$ values than odd cycles.
	Flatband	Possible. Gapped as a function of momenta ( $k$ ), & for 2 (or, more) coins.	Possible. Gapped as a function of momenta ( $k$ ), & for 2 (or, more) coins.
	Rotational flatband	Not possible.	Possible, occurs when $D \geq 2$ .
	Topological Winding number	Fractional & topological ( $\omega = \pm\frac{1}{2}$ )(Two values, with phase transitions).	Fractional & topological ( $\omega = \pm\frac{1}{2}$ )(Two values, with phase transitions).
	Edge states	Possible.	Possible.

TABLE II. A comparative analysis of the topological characteristics across the SCSS-CQW protocols: step-independent single coin split-step CQW (SI-SCSS-CQW) and step-dependent single coin split-step CQW (SD-SCSS-CQW), for different cycles (with even and odd number of sites).

small to moderate levels of dynamic and static coin disorder as well as against topological-phase preserving perturbations, see SM Sec. 1.D. We also model the decay of survival probabilities of the edge states vs time (with and without disorder) and show the long-time stability of the generated edge states (also, see SM Sec. II). These findings provide a versatile and experimentally accessible platform to realize and control fractional winding numbers, topological flat-bands and robust edge-states in synthetic quantum systems, thereby opening unprecedented pathways towards fault-tolerant-quantum-computing, robust quantum state transfer and quantum engineering.

**SUPPLEMENTARY MATERIAL**

This material provides additional details and results for single-coin split-step cyclic quantum walks (SCSS-CQW), supporting the key findings of the main text. In Sec. I, for the SCSS-CQW evolution, we derive energy dispersion, group velocity, and generic winding number which characterizes its topological phases. We then analytically derive the conditions on rotation angles and step-dependency parameters, for the occurrence of gapped flat-bands. These are then validated with vanishing group-velocity (both analytically & numerically). The numerical results of energy dispersion as well as topological phases (with fractional winding-numbers) with step-dependent variant and step-independent variant of SCSS-CQW for 7,8-cycle graphs are then put forth. We numerically demonstrate the resilience of the generated edge-states against gate disorder as well as phase-preserving perturbations. In section II, we model the decay of survival probabilities vs time, and show the long-time stability of the generated edge states. Finally, Sec. III provides an algorithm for plotting probability distribution and edge state generation via the SCSS-CQW protocol.

**I. ENERGY DISPERSION AND TOPOLOGICAL PHASES WITH SINGLE-COIN SPLIT-STEP CYCLIC QUANTUM WALK (SCSS-CQW)**

**A. Energy dispersion and topological winding numbers**

The time-evolution of a quantum particle with a single-coin split-step CQW (SCSS-CQW) is governed by the evolution operator,

$$\hat{U}_{evo} = \hat{S}_+ \hat{C}_\gamma \hat{S}_- \hat{C}_\gamma, \quad (6)$$

where the shift operators are:

$$\hat{S}_+ = \sum_{n=0}^{N-1} |0\rangle_c \langle 0|_c \otimes (|x+1\rangle \langle x| + |1\rangle_c \langle 1|_c \otimes |x\rangle \langle x|),$$

$$\hat{S}_- = \sum_{n=0}^{N-1} |0\rangle_c \langle 0|_c \otimes (|x\rangle \langle x| + |1\rangle_c \langle 1|_c \otimes |x-1\rangle \langle x|),$$

where  $N$  is the number of sites of the cyclic graph, and the coin operator:

$$\hat{C}_\gamma = e^{-i\Delta \cdot \gamma \cdot \sigma_y}. \quad (7)$$

In Eq. (7),  $\Delta = \frac{D}{2}$  and  $D$  being an integer.  $D = 1$  refers to no step dependency in coin operation while  $D \geq 2$ , i.e.,  $D = 2, 3, 4, \dots$  refers to a step-dependent coin. We consider the Fourier transform (FT) of the position basis, that is,  $|k'\rangle = (\frac{1}{\sqrt{N}}) \sum_{x=0}^{N-1} e^{i(\frac{2\pi}{N})xk'} |x\rangle_p$ . The parameters  $k', x \in \{0, 1, 2, \dots, N-1\}$ . Substituting  $\omega_N = e^{\frac{2\pi i}{N}}$ , we can write,

$$\hat{S}_+ |0\rangle_c |k'\rangle = \omega_N^{-k'} |0\rangle_c |k'\rangle, \quad \hat{S}_+ |1\rangle_c |k'\rangle = \omega_N^0 |1\rangle_c |k'\rangle,$$

$$\text{i.e., } \hat{S}_+ = \sum_{k'} \begin{pmatrix} \omega_N^{-k'} & 0 \\ 0 & 1 \end{pmatrix} \otimes |k'\rangle \langle k'|. \quad (8)$$

Similarly,

$$\hat{S}_- |0\rangle_c |k'\rangle = \omega_N^0 |0\rangle_c |k'\rangle, \quad \hat{S}_- |1\rangle_c |k'\rangle = \omega_N^{k'} |1\rangle_c |k'\rangle, \\ \text{i.e., } \hat{S}_- = \sum_{k'} \begin{pmatrix} 1 & 0 \\ 0 & \omega_N^{k'} \end{pmatrix} \otimes |k'\rangle \langle k'|. \quad (9)$$

In terms of Pauli matrices, we arrive at,

$$\hat{S}_+ = e^{-i(\frac{2\pi k'}{2N})(\sigma_z + \mathbf{1})}, \quad \hat{S}_- = e^{-i(\frac{2\pi k'}{2N})(\sigma_z - \mathbf{1})}. \quad (10)$$

With the stroboscopic evolution,  $\hat{U}_{evo} = e^{-i(\hat{H})}$ ,  $\hat{H} = \vec{\sigma} \cdot \hat{n} * E(k)$ ,  $k = \frac{2\pi k'}{N}$ ; we obtain,

$$\hat{U}_{evo} = \hat{S}_+ \hat{C}_\gamma \hat{S}_- \hat{C}_\gamma = e^{-iE(k)\vec{\sigma} \cdot \vec{n}}, \quad (11)$$

from which we calculate energy dispersion to be,

$$\cos E = [\cos k(\cos(\Delta \cdot \gamma))^2 - (\sin(\Delta \cdot \gamma))^2], \\ \text{or, } E_\pm = \pm \cos^{-1} [\cos k(\cos(\Delta \cdot \gamma))^2 - (\sin(\Delta \cdot \gamma))^2]. \quad (12)$$

Clearly, one can draw the following conclusion from the energy dispersion (Eq. (12)):

1.  $(\cos(\Delta \cdot \gamma))^2 = 0$ , implies that the energy bands become  $k$ -independent and we see symmetric flat bands.
2.  $-(\sin(\Delta \cdot \gamma))^2 = 0$ , leads to the possibility for linear energy gap closing, for SCSS-CQW in  $N \rightarrow$  large limit. This is similar to what is seen in CQW, see Ref. [43].

The group velocity ( $V_{gr}$ ) can be calculated from Eq. (12), i.e.,

$$V_{gr} = \pm \frac{\sin k(\cos(\Delta \cdot \gamma))^2}{\sqrt{1 - [\cos k(\cos(\Delta \cdot \gamma))^2 - (\sin(\Delta \cdot \gamma))^2]^2}}, \quad (13)$$

and the effective mass ( $m^* = \frac{\hbar^2}{\partial_k V_{gr}}$ ) of the particle in the units of  $\hbar = 1$  is,

$$m^* = \pm \frac{16(\sec(\gamma\Delta))^2 \left(1 - (\cos(k)(\cos(\gamma\Delta))^2 - (\sin(\gamma\Delta))^2)\right)^{3/2}}{\cos(k)(8 - 8(\cos(\gamma D))^2) + 2(\cos(2k) + 3)(\sin(\gamma D))^2}, \quad (14)$$

where, + (-) signs correspond to the upper (lower) energy bands. As shown in Eqs. (13)-(14), the group velocity and effective mass can be controlled by two parameters: rotation-angle  $\gamma$  and step-dependency parameter  $D$ . These quantities provide a check on flat band formation, i.e., the group velocity vanishes for flat bands, also see Sec. B and Fig. 6 below for further details. These are also useful in determining diffusion rates, carrier mobility and wave-packet-spreading in the case of a solid state quantum-system, see Refs. [56–58]. From the stroboscopic evolution, given in Eq. (11), we get the components of the winding vector  $\vec{n}(k)$ ,

$$\vec{n}(k) = \frac{1}{\sin E(k)} \begin{bmatrix} -\sin k \cos(\Delta.\gamma) \sin(\Delta.\gamma) \\ \cos k \cos(\Delta.\gamma) \sin(\Delta.\gamma) + \sin(\Delta.\gamma) \cos(\Delta.\gamma) \\ \sin k (\cos(\Delta.\gamma))^2 \end{bmatrix} \quad (15)$$

Finally, the winding number (see Eq. (1) of main) for a discretized system of a  $N$ -cycle graph reads,

$$\omega_{\gamma,D,N} = \frac{1}{2\pi} \sum_{k'=0}^{N-1} \left( \vec{n} \times \frac{\partial \vec{n}}{\partial k'} \right) \cdot \hat{A}, \quad (16)$$

where the unit vector,  $\hat{A}(\gamma, D) = (\cos(\Delta.\gamma), 0, \sin(\Delta.\gamma))$  and  $\Delta = \frac{D}{2}$ . Thus, we get the winding numbers,  $\omega_{\gamma,D,N} = \frac{Z_{\gamma,D,N}}{\pi}$  to be,

$$\omega_{\gamma,D,N} = \sum_{k'=0}^{N-1} -\frac{2 \sin(\gamma\Delta)}{N \left( 2 \cos^2\left(\frac{k}{2}\right) \cos(\gamma D) + \cos(k) - 3 \right)}. \quad (17)$$

For example, for step-independent SCSS-CQW, i.e.,  $D = 1$  and  $\gamma = \frac{\pi}{2}$  for  $N = 3, 4, 7, 8$  sites, the winding numbers are,  $\omega_{\frac{\pi}{2},1,N} = 0.505076, 0.500867, 0.500004, 0.500001$ , which for  $N \rightarrow$  very large, i.e.,  $N = 1000$  gives  $\omega_{\frac{\pi}{2},1,1000} = \frac{1}{2} = 0.5$ . Similarly for  $D = 5$ , i.e., a step-dependent SCSS-CQW, with  $\gamma = \frac{\pi}{2}$  and  $N = 3, 4, 7, 8$  site cyclic graphs, we obtain winding numbers to be,  $\omega_{\frac{\pi}{2},2,N} = -0.505076, -0.500867, -0.500004, -0.500001$ , which for  $N \rightarrow$  very large, i.e.,  $N = 1000$ , gives  $\omega_{\frac{\pi}{2},2,1000} = -\frac{1}{2} = -0.5$  (almost the same as small cyclic graphs). Studying topological effects with smaller cyclic graphs is reasonable, i.e., it gives identical results to larger graphs but with much less resource expenditure (see, Sec. IV below), as was also seen in Ref. [43] for CQW.

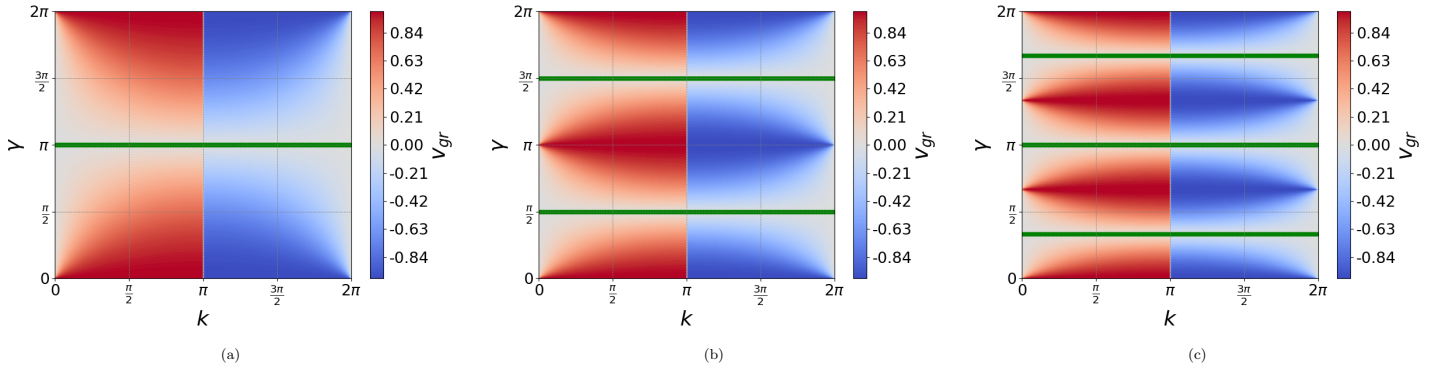


Figure 6. Group velocity (see, Eq. (13)) as a function of quasimomentum  $k$  (for infinite site cyclic graphs) and coin rotation-angle  $\gamma$  for SCSS-CQW evolution with (a) SI coin  $D = 1$ , and SD coins (b)  $D = 2$  and (c)  $D = 3$ . **Flat bands**, where the energy  $E(k)$  is not dependent on momenta  $k$ , and are characterized by 0 group velocity (that is,  $V_{gr} = 0$ , for all  $k$ ), consistent with condition of Eq. (20) and marked in solid green-lines. The flat bands forms in (a) at  $\gamma = \pi$ ; (b) at  $\gamma = \frac{\pi}{2}, \frac{3\pi}{2}$ ; and (c) at  $\gamma = \frac{\pi}{3}, \pi, \frac{5\pi}{3}$ .

## B. Flat bands and group velocity

We show gapped flat-bands can be generated via SCSS-CQW by tuning the rotation angles and the step-dependency parameter  $D$  in the SCSS-CQW evolution.

As derived in main Eq. (2) and Eq. (12), the energy dispersion for SCSS-CQW in the cyclic graph of site  $N$  is,

$$E_{\pm} = \pm \cos^{-1} \left[ \cos k (\cos(\Delta.\gamma))^2 - (\sin(\Delta.\gamma))^2 \right] \quad (18)$$

From the above equation, it is evident that symmetric energy flat bands are obtained for,

$$\cos(\Delta \cdot \gamma) = 0, \quad (19)$$

i.e., energy  $E_{\pm}$  becomes  $k$  or  $k'$  independent, i.e.,

$$\Delta \cdot \gamma = (2n + 1) \frac{\pi}{2}, \text{ or, } \gamma = \frac{(2n + 1)\pi}{D} \quad (20)$$

where  $n \in \mathbb{Z}_+ \cup \{0\}$ .

The condition in Eq. (20) is for flat bands, which may be gapped or gapless. With the above condition (20) satisfied, to get gapless flat-bands, one requires,

$$E_{\pm} = \pm \cos^{-1} [-\sin^2(\Delta \cdot \gamma)] = 0, \text{ or, } \sin^2(\Delta \cdot \gamma) = -1, \quad (21)$$

which is not a valid statement. Thus, gapless flat-bands can not be generated via SCSS-CQW, although gapped flat-bands manifest in SCSS-CQW evolution for  $\gamma = \frac{(2n+1)\pi}{D}$ , see Eq. (20).

For example, for  $D = 1$  at  $\gamma = \pi$  ( $n = 0$ ), for  $D = 2$  at  $\gamma = \frac{\pi}{2}, \frac{3\pi}{2}$ , SCSS-CQW yields flat bands, see Eq. (20) and Fig. 2 in main.

gapped flat-bands are due to vanishing group velocity at  $\gamma$  values derived in Eq. (20). One can observe this analytically, from group velocity given in Eq. (13), Plugging the  $\gamma$  values of Eq. (20), the numerator of Eq. (13) vanishes and thus, group velocity  $V_{gr}$  vanishes too, and this occurs at all flat bands. This is plotted numerically in Fig. 6, where we see group velocity vanish (green lines) as predicted analytically.

### C. Numerical analysis: Energy spectrum and topological phase structure of the SCSS-CQW

Band dispersion and topological invariant (winding number,  $\omega$ ) as a function of the rotation angle  $\gamma$  (Eqs. (12), (17)), are shown in Fig. 7 for SI coin ( $D = 1$ ), and Figs. 8 for step-dependent (SD) coin ( $D = 3$ ) for  $N = 7, 8$ -site cyclic graphs. Both SD and SI SCSS-CQW host conducting (energy gap closing) and insulating phases.

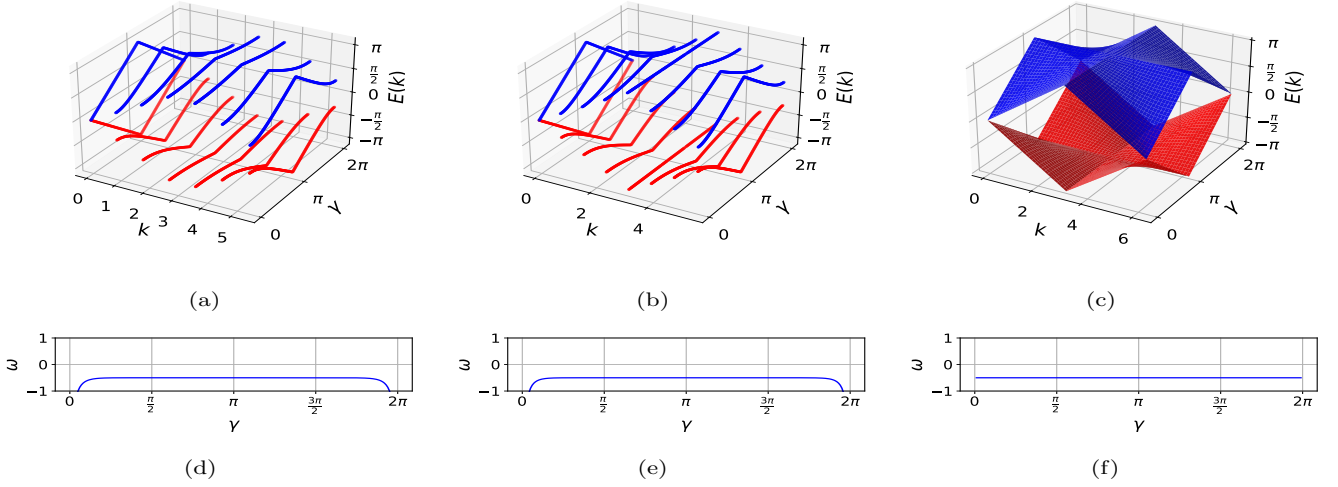


Figure 7. The spectrum of energy ( $E(k)$ ) as a function of  $k$  & coin-angle ( $\gamma$ ) with: (a) 7-cycle; (b) 8-cycle; (c) 1000-cycle. Red (blue) curves denote the upper (lower) quasienergy branches. (d)–(f) Corresponding winding number  $\omega$  plotted against  $\gamma$  for 7-cycle, 8-cycle, and 1000-cycle, respectively, via the SI SCSS-CQW protocol with  $D = 1$ .

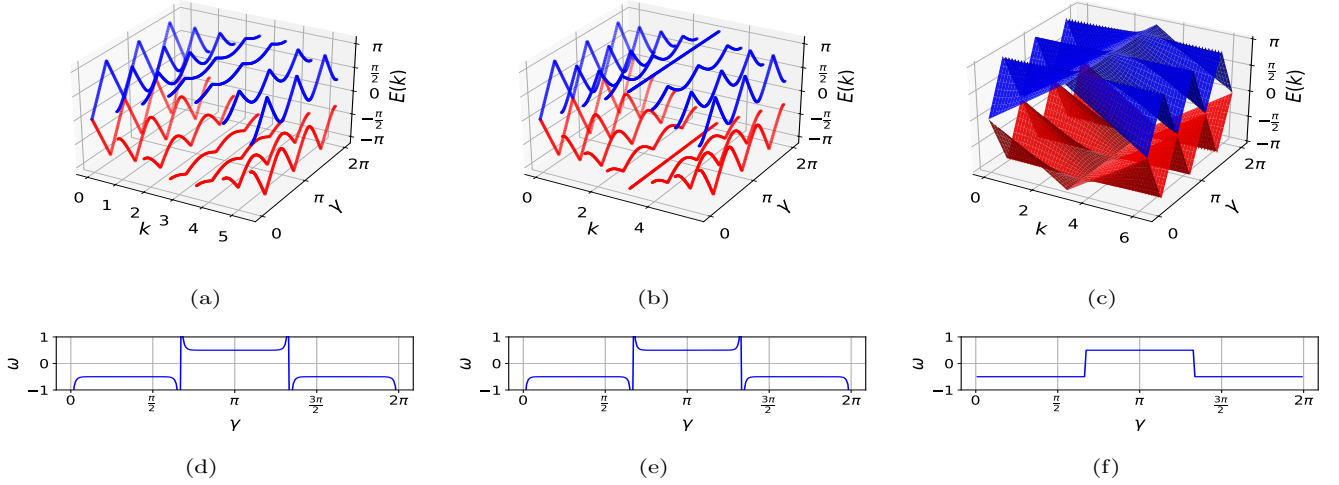


Figure 8. The spectrum of energy ( $E(k)$ ) as a function of  $k$  & coin-angle ( $\gamma$ ) with: (a) 7-cycle; (b) 8-cycle; (c) 1000-cycle. Red (blue) curves denote the upper (lower) quasienergy branches. (d)–(f) Corresponding winding number  $\omega$  plotted against  $\gamma$  for 7-cycle, 8-cycle, and 1000-cycle, respectively, for the SD SCSS-CQW protocol with  $D = 3$ .

#### D. Resilience of edge states against coin disorder (dynamic-static) & minor phase-preserving-perturbations

Here, we numerically investigate the effect of coin (gate) disorder (dynamic and static), and minor phase-preserving perturbations on the generated topological edge states generated using the SCSS-CQW evolution, see Fig. 3 of main.

*Dynamic coin disorder*– We examine the role of dynamic coin (gate) disorder in the SCSS-CQW dynamics and on the generated edge states with dynamic disorder of strength  $\Delta$ . Here, the site dependent rotation-angle  $\gamma_x$  required to generate topological phases, and topological edge states is modified as [43, 53],

$$\gamma_x \rightarrow \gamma_x + \Delta \delta(t),$$

the random fluctuations (site-independent)  $\delta(t) \in [-\pi, \pi]$  are chosen at each time step, with the total number of random values matching the evolution time. For a specific realization, these random values are drawn from a uniform distribution. To evaluate the probability of finding the walker at a given site  $x$ , i.e.,  $P(x)$ , we average over 500 such realizations. For more technical details on the implementation of dynamic coin disorder in quantum walk dynamics, see Refs. [43, 53]. The case  $\Delta = 0$  corresponds to a clean system without any dynamic coin disorder. As discussed in Fig. 3 of main, a topological edge state emerges localized at the lattice site  $x = 0$ , due to a phase boundary created by 2 different coin rotation angles:  $\gamma = \frac{6\pi}{4}$  (applied to position site 0 and winding number:  $\omega = \frac{1}{2}$ ) and  $\gamma = \frac{3\pi}{4}$  (applied to the other position

sites and winding number:  $\omega = -\frac{1}{2}$ ), see Fig. 9(a), where the probability at position site 0 remains significant and persists over time. Figs. 9(b) and (c) illustrate how dynamical coin disorder with degrees of disorder:  $\Delta \rightarrow 0.01$ , and  $\Delta \rightarrow 0.050$ , influences the emergent localized edge state (Fig. 9(a)). The results indicate that the generated edge states remain stable under weak dynamic-coin disorder within the range  $0 < \Delta \lesssim 0.05$ . In contrast, for stronger disorder, i.e.,  $\Delta \gtrsim 0.05$ , the resulting edge-state probability distribution becomes significantly perturbed.

*Static coin disorder*– We now examine the role of static coin disorder [43], in SCSS-CQW dynamics and on the edge states, with the strength of disorder  $s$ . In this case, the site-dependent coin rotation-angle  $\gamma_x$ , where the subscript  $x$  labels the position sites, responsible for generating the topological phases and topological edge states, is modified as [43],

$$\gamma_x \rightarrow \gamma_x + s \delta_x.$$

$\delta_x$  takes random values in  $[-\pi, \pi]$  and is sampled uniformly with the sample size equal to the site number in the cycle graph. Each realization of disorder is taken independently.  $s = 0$  corresponds to a completely disorder-free SCSS-CQW evolution.

In Fig. 3 of main, we discussed the appearance of an edge-state (topological) at the position-site: 0, when 2 different topological phases are interfaced, characterized by the coin rotation angles  $\gamma = \frac{6\pi}{4}$  (applied to the position site 0 and winding number:  $\omega = \frac{1}{2}$ ) and  $\gamma = \frac{3\pi}{4}$  (applied to the other position sites and the winding number,  $\omega = -\frac{1}{2}$ ) (see Fig. 10(a)). From the illustrated edge state in the Fig. 10 (a), the particle's probability at the position site  $x = 0$  remains non-vanishing for a large long number of time-steps  $t$  for zero disorder.

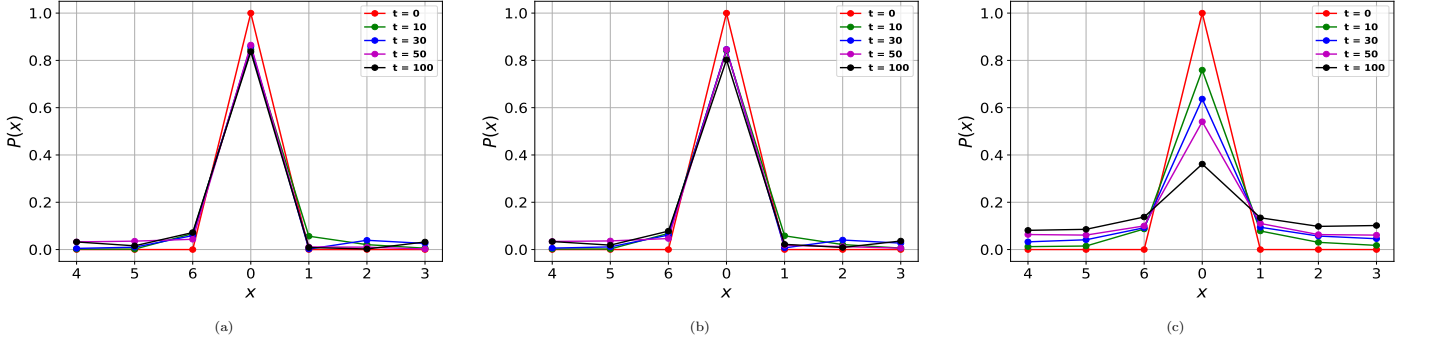


Figure 9. (a) The probability profile ( $P(x)$ ) for position sites demonstrating an edge-localized state at  $x = 0$ , generated by a junction of two topological sectors characterized by winding numbers  $\omega = \frac{1}{2}$  ( $\gamma = \frac{6\pi}{4}$ ) and  $\omega = -\frac{1}{2}$  ( $\gamma = \frac{3\pi}{4}$ ), for the SD SCSS-CQW protocol ( $D = 2$ ) on a seven-site cycle in the disorder-free limit. (b) Modification of the localized edge profile under dynamic-coin randomness with strength  $\Delta = 0.01$ . (c) Corresponding behavior for stronger dynamic-coin randomness  $\Delta = 0.05$ . In panels (b) and (c), results are obtained by ensemble averaging over 500 statistically independent disorder instances; dynamic-coin simulations require greater computational effort compared to the static-coin scenario.

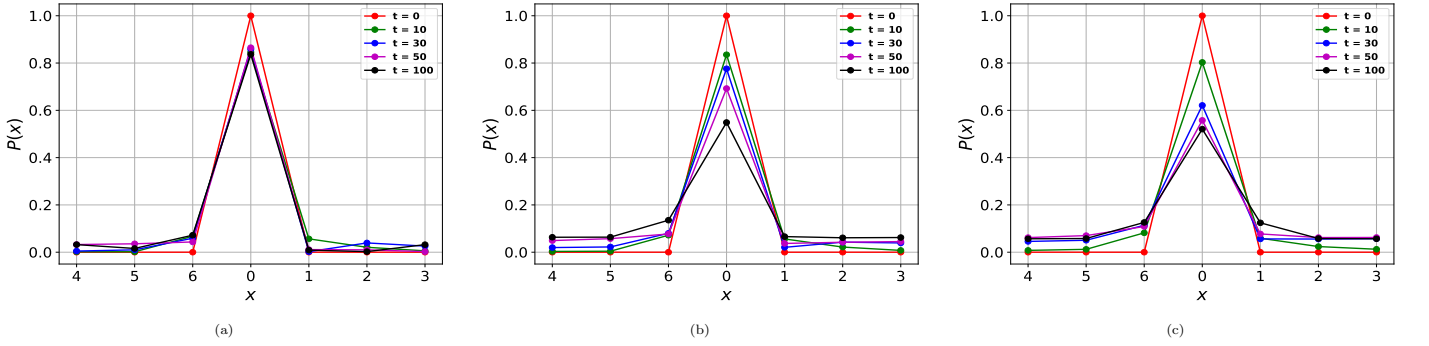


Figure 10. (a) The probability profile ( $P(x)$ ) for position sites showing localization at  $x = 0$  (edge state), induced by an interface between 2 topological phases characterized by  $\omega = \frac{1}{2}$  ( $\gamma = \frac{6\pi}{4}$ ) and  $\omega = -\frac{1}{2}$  ( $\gamma = \frac{3\pi}{4}$ ), for the SD SCSS-CQW protocol ( $D = 2$ ) on a seven-site cycle in the absence of disorder. (b) Modification of the localized state under static-coin randomness with strength  $s = 0.025$ . (c) Corresponding behavior for stronger static-coin randomness  $s = 0.05$ . In panels (b) and (c), results are obtained from an ensemble of 1000 independent disorder realizations, and  $P(x)$  represents the ensemble-averaged distribution.

Figs. 10(b) and (c) illustrate the response of the localized edge state to static-coin noise (disorder) with disorder degrees  $s = 0.025$  and  $s = 0.05$ , respectively, relative to the disorder-free case of Fig. 10(a). Our numerical analysis confirms the robustness of the corresponding topological feature.

Our numerical results indicate the resilience of this topological edge state against small static-coin disorder, since the probability at site 0 does not decrease noticeably with disorder. However, for stronger disorder ( $s \gtrsim 0.05$ ) the amplitude of the edge state becomes significantly altered.

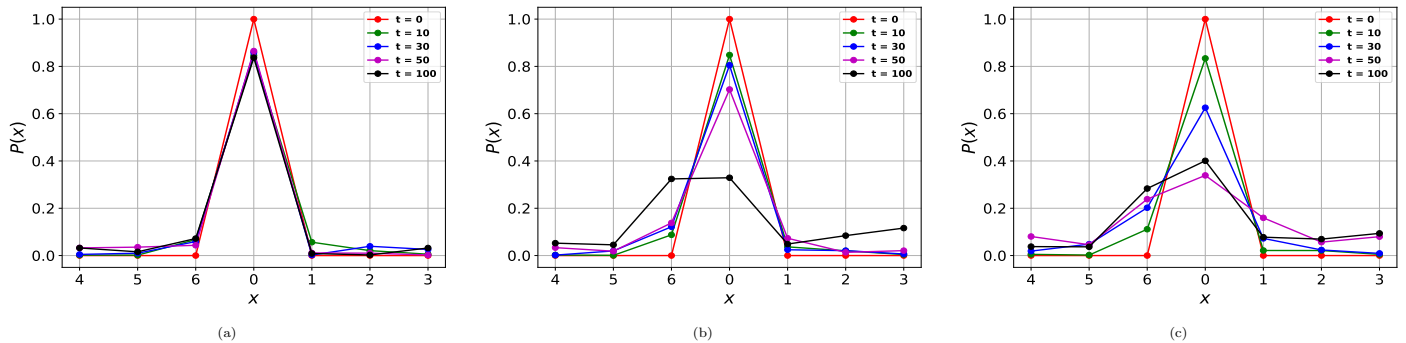


Figure 11. (a) The probability profile ( $P(x)$ ) for position sites, highlighting the edge state localized at site  $x = 0$ , appearing at boundary between two different topological phases ( $\omega = \frac{1}{2}$  with  $\gamma = \frac{6\pi}{4}$ ,  $\omega = -\frac{1}{2}$  with  $\gamma = \frac{3\pi}{4}$ ), for SD SCSS-CQW ( $D = 2$ ) in a 7-cycle graph. (b) Persistence of topological edge state due to small phase-preserving perturbations, i.e., edge state at phase boundary between the 2 topological phases:  $\omega = \frac{1}{2}$  ( $\gamma = \frac{6.05\pi}{4}$ ) and  $\omega = -\frac{1}{2}$  ( $\gamma = \frac{3\pi}{4}$ ). (c) Persistence of topological edge state under small phase-preserving perturbation, i.e., edge state at the boundary between 2 topological phases:  $\omega = \frac{1}{2}$  ( $\gamma = \frac{6.1\pi}{4}$ ) and  $\omega = -\frac{1}{2}$  ( $\gamma = \frac{3\pi}{4}$ ).

*Phase-preserving disorder.*— Phase-preserving perturbations [2] can be introduced by altering the rotation angles ( $\gamma$ ) by a small amount that defines the topological phases as well as topological edge states via the protocol: SCSS-CQW dynamics, without affecting the winding number ( $\omega$ ). For instance,  $\gamma = \frac{6\pi}{4}$ ,  $\gamma = \frac{6.05\pi}{4}$  and  $\gamma = \frac{6.1\pi}{4}$ , corresponds to the same winding number  $\omega = \frac{1}{2}$ . By switching the rotation-angle from  $\frac{6\pi}{4}$  to  $\gamma = \frac{6.05\pi}{4}$  or  $\gamma = \frac{6.1\pi}{4}$ , the topological invariant, namely the winding number, remains unchanged. In Fig. 4 of the manuscript as well as in Fig. 11(a) referenced above, we demonstrate that a localized edge state arises at the lattice site  $x = 0$  when a phase boundary is engineered by employing two distinct coin parameters:  $\gamma = \frac{6\pi}{4}$  at the site 0 (corresponding to the winding number,  $\frac{1}{2}$ ) &  $\gamma = \frac{3\pi}{4}$  at the remaining sites (corresponding to winding number  $-\frac{1}{2}$ ). This results in a pronounced position probability at position site 0 that remains stable over a very long time, indicating a long-lived and stable edge state. In Figs. 11(b)-(c), the perturbation is introduced by changing the coin rotation-angle at site 0 from  $\frac{6\pi}{4}$  to  $\frac{6.05\pi}{4}$  and  $\frac{6.1\pi}{4}$ , corresponding to winding number  $\frac{1}{2}$ . Interestingly, the observed edge state remains almost unaffected under such weak perturbations (phase preserving), since the position site probability (at the site 0), does not decay significantly or vanish over time. However, a larger deviation in  $\gamma$  value has a relatively larger impact on the edge state amplitude, see Figs. 11(b)-(c).

## II. TEMPORAL STABILITY OF THE EDGE STATE

### A. Ideal

We have demonstrated the presence of a localized edge-state in the SCSS-CQW protocol (see, Fig. 4(c) of main). We now analyze the temporal stability of this edge state by examining the time dependence of the survival probability of the edge site.

At each discrete time step  $t$ , we extract the probability of edge state, as,

$$P(x = 0) \equiv \sum_{c=0,1} |\langle x = 0, c | \psi(t) \rangle|^2, \quad (22)$$

which quantifies the probability of finding the walker at site  $x = 0$ . The behavior of  $P(x = 0)$  serves as a sensitive diagnostic of edge state localization and transport properties of the system.

We plot in Fig. 12(a),  $P(x = 0)$  as a function of time. A rapid decay of this quantity would indicate delocalization or leakage of the walker away from the edge, whereas saturation to a finite value would signal robust localization. This plot would therefore provide a direct visualization of the persistence of the edge state.

Indeed, in Fig. 12, we see a saturation of  $P(x = 0)$  near 0.85. We employ Mathematica's built-in `FindFormula` and `FindFit` to infer an analytical function that best describes the numerical data  $\{t, P(x = 0)\}$ .

Applying `FindFormula` to the ideal (disorder-free) data yields a constant function i.e.,  $P(x = 0) = 0.845071$ . Importantly, the inferred formula does not contain any exponential factors of the form  $e^{-\gamma t}$  or power-law terms  $t^{-\alpha}$ . The resulting fit reproduces the numerical data with a root-mean-square error (RMSE)  $\approx 0.04$ , demonstrating excellent agreement over the considered time window.

The absence of any systematic decay term in the data-driven fit confirms that the edge-state survival probability saturates to a finite value ( $\sim 0.85$ ) and remains dynamically stable up to long simulated times. This provides strong evidence that the observed edge state is not transient but represents a robust, long-lived localized mode for ideal SCSS-CQW dynamics.

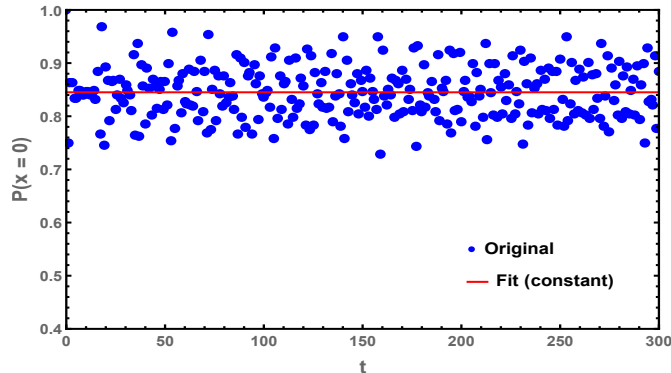


Figure 12. Edge-state survival probability  $P(x=0)$  vs timestep  $t$  using SD SCSS-CQW ( $D=2$ ) on a 7-cycle graph, without any disorder (**ideal case**). The numerical data exhibit fluctuations around a constant mean value, and are well captured by a constant fit (red), demonstrating long-time saturation and the stability of the localized edge state.

### B. Dynamic disorder

In the previous Sec. I.D, we studied the resilience of emergent edge states against dynamic coin disorder, then static coin disorder (see, Figs. 9, 10), and finally the phase-preserving perturbations (see, Figs. 11). Below, we provide the time dependence of the edge state under disorder with the same strength of disorder taken in Sec. I.D and Figs. 9, 10 and 11. We utilize Mathematica’s built-in `FindFormula` to analyze the behaviour of the edge-state survival probability under small to moderate level of disorder.

Under small dynamic-coin disorder of strength  $s = 0.01$ , we analyse the decay of the edge-site survival probability  $P(x=0)$ , as shown in Fig. 13. The decay of the edge-state probability is very slow, indicating a high degree of robustness against weak temporal fluctuations in the coin parameters. Applying `FindFormula` to the data, we find a linear function  $0.843358 - 0.00031128t$  fits the data with RMSE 0.042, demonstrating excellent agreement over the entire time window. We conclude that under small dynamical disorder, the observed edge state is robust and long-lived, exhibiting very slow decay.

We repeat the same analysis for a stronger dynamical coin disorder of strength  $s = 0.05$ , shown in Fig. 14. In this case, applying `FindFormula` and `FindFit` to the data, we find the cubic function,  $0.8342 - 0.0068t + 0.000026t^2 + -3.8143 * 10^{-8}t^3$  fits the data with RMSE 0.0196, demonstrating excellent agreement over the en-

tire time window. In this case, the edge-state survival probability decays faster compared to the small dynamic disorder case. Nevertheless, the decay remains slow enough for the edge state to remain well localized up to intermediate times ( $t \lesssim 100$ ), as evident from Fig. 14.

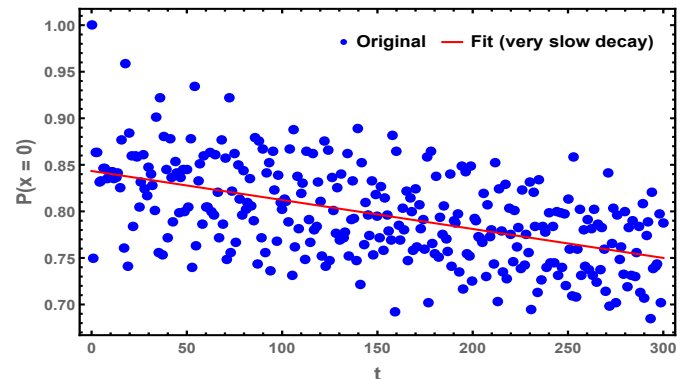


Figure 13. Edge-state survival probability  $P(x=0)$  vs timestep  $t$  using SD SCSS-CQW ( $D=2$ ) on a 7-cycle graph, under small **dynamical disorder** of strength  $s = 0.01$ . The numerical data exhibit a linear fit (red) with very slow decay, demonstrating long-time stability of the localized edge state.

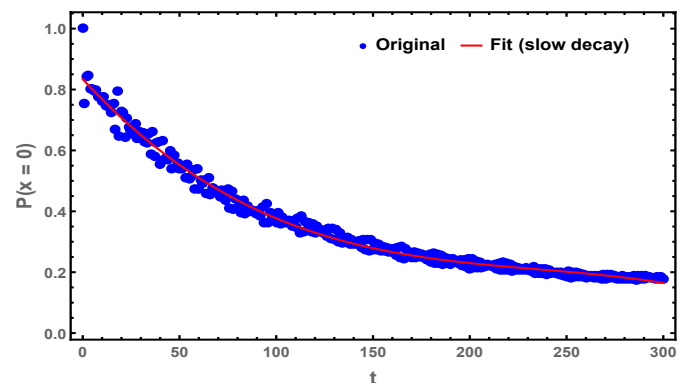


Figure 14. Edge-state survival probability  $P(x=0)$  versus timestep  $t$  using SD SCSS-CQW ( $D=2$ ) in 7-cycle graph, under large **dynamical disorder** of disorder strength:  $s = 0.05$ . The numerical data exhibit a cubic fit (red) with slow decay, demonstrating long-time stability of the localized edge state.

### C. Static disorder

In Sec. I.D, we have demonstrated that the generated edge states remain robust under static coin disorder (see Fig. 10). Here, we analyze the explicit time dependence of the edge-state survival probability for the same disorder strengths considered in Sec. I.D. In particular, we study the behavior of the edge-site probability  $P(x=0)$  under static disorder using Mathematica’s built-in `FindFormula` and `FindFit` to identify effective functional descriptions of the numerical data.

Under small static-coin disorder with degree of disorder  $s = 0.025$ , the resulting edge-site survival probability  $P(x = 0)$  exhibits a slow oscillatory decay over the entire simulated time window, as shown in Fig. 15. Applying `FindFormula` and `FindFit` to the data, we find a quartic polynomial,  $0.936895 - 0.00904871t + 0.0000830043t^2 - 3.16 \times 10^{-7}t^3 + 4.24 \times 10^{-10}t^4$  provides the best description, with an RMSE of  $\approx 0.031$ . This confirms that the edge state remains dynamically stable for an appreciable amount of time and exhibits a slow oscillatory decay, under small static disorder.

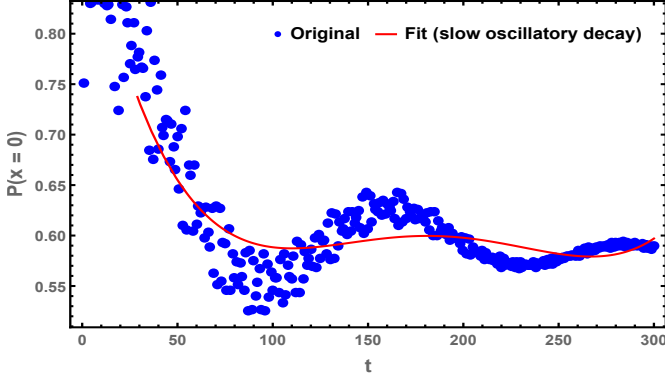


Figure 15. Edge-state survival probability  $P(0)$  as a function of the time step  $t$ , using SD SCSS-CQW ( $D = 2$ ) on 7-cycle graph, in the presence of small **static-coin disorder** with strength of disorder,  $s = 0.025$ . This numerical data can be fitted with a quartic polynomial fit (red) with slow oscillatory decay, demonstrating long-time stability of the localized edge state.

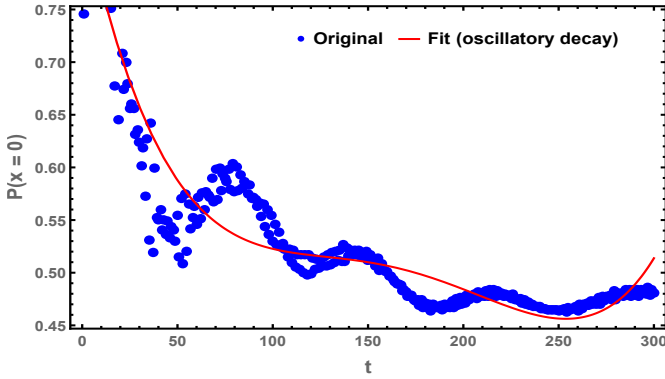


Figure 16. Edge-state survival probability ( $P(x = 0)$ ) versus timestep  $t$  using SD SCSS-CQW ( $D = 2$ ) on 7-cycle graph, in the presence of strong **static-coin disorder** with strength  $s = 0.05$ . This numerical data can be fitted with a quartic polynomial fit (red) and exhibits an oscillatory decay, which demonstrates long-time stability of the localized edge state.

We repeat the same analysis for a stronger static disorder of coin-disorder strength:  $s = 0.05$ , shown in Fig. 16. In this case, the edge-site survival probability  $P(x = 0)$  exhibits a slightly faster decay over the simulated time

window compared to the small static disorder case, as shown in Fig. 16. Applying `FindFormula` and `FindFit` to the data, we again find that a quartic polynomial,  $0.847531 - 0.00846569t + 0.0000812807t^2 - 3.42 \times 10^{-7}t^3 + 5.093 \times 10^{-10}t^4$  provides the best description, with an RMSE of  $\approx 0.029$ . This confirms that the edge state remains dynamically stable for a slightly shorter time as compared with the small static disorder case, and exhibits an oscillatory decay. This indicates that static disorder does not induce delocalization of the edge state even at higher disorder strengths. These results demonstrate that the edge state generated in the SCSS-CQW protocol is quite robust against static coin disorder and remains unaffected over a long evolution time.

#### D. Phase-preserving perturbations

We plot in Figs. 17 and 18 the time dependence of the edge-site survival probability  $P(x = 0)$  under two representative phase-preserving perturbations considered in Figs. 11(b) and 11(c), respectively. As in the previous cases, we analyze the long-time behavior of the edge state by fitting the numerical data using Mathematica's built-in `FindFormula` and `FindFit`. In the plot in Figs. 17 and 18, the time dependence of the edge-site survival probability  $P(x = 0)$  can be fitted with a quartic polynomial fit,  $0.843556 + 0.00417343 * t - 0.000169219 * t^2 + 1.08346 * 10^{-6} * t^3 - 1.8982 * 10^{-9} * t^4$  (with RMSE  $\approx 0.095$ ) and a sextic polynomial fit,  $0.906483 + 0.00445627 * t - 0.000829577 * t^2 + 0.0000161687 * t^3 - 1.22093 * 10^{-7} * t^4 + 4.01832 * 10^{-10} * t^5 - 4.82202 * 10^{-13} * t^6$  (with RMSE  $\approx 0.1$ ). In the case of Fig. 17, the survival probability remains finite and exhibits bounded oscillations without any systematic decay, indicating robustness of the edge state against phase-preserving perturbations, while in Fig. 18 it exhibits an slow oscillatory decay. In both cases, the edge states shows robustness against phase-preserving perturbations for a quite long time.

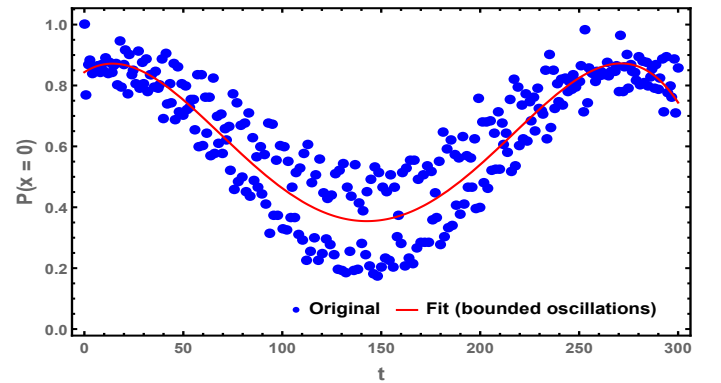


Figure 17. Edge-state survival probability  $P(x = 0)$  vs timestep  $t$  using SD SCSS-CQW ( $D = 2$ ) on 7-cycle graph, under small phase-preserving perturbations as in Fig. 11(b). The numerical data is fitted with quartic polynomial fit (red), demonstrating long-time stability of the localized edge state.

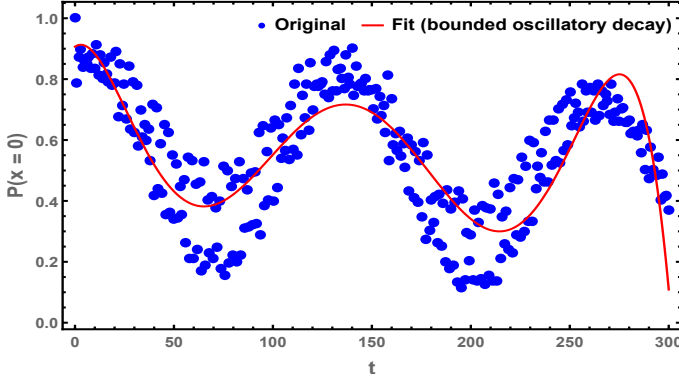


Figure 18. Edge-state survival probability  $P(x=0)$  vs time-step  $t$  using SD SCSS-CQW ( $D=2$ ) on 7-cycle graph, under small phase-preserving perturbations as in Fig. 11(c). The numerical data is fitted with a sextic polynomial fit (red), demonstrating slow oscillatory decay (long-time stability of the localized edge state).

### III. ALGORITHM FOR EDGE STATE GENERATION VIA SCSS-CQW

Below, we outline the algorithm, i.e., steps to generate quantum-walk dynamics and edge-state using a *single-coin split-step cyclic quantum walk* (SCSS-CQW) on a  $N$ -cycle graph (see Fig. 4(a)).

**Require:** Total number of time steps  $T$

**Require:** Number of lattice sites  $N$  (cyclic graph:  $x = 0, 1, \dots, N-1$ )

**Require:** Single-coin operator  $\hat{C}_\gamma$  (Eq. (7)). Choosing coin  $\hat{C}_\gamma$  at site  $x=0$  and  $\hat{C}_\gamma$  at sites  $x \in \{1, N-1\}$  with two different winding numbers (Eq. (17))

**Require:** Conditional shift operators  $\hat{S}_+$  and  $\hat{S}_-$  (Eq. (10))

**Require:** Initial walker state  $|\psi(0)\rangle$

**Ensure:** Position probability distribution:  $\text{prob}[t][x]$  at time-step  $\tau = 0, 1, 2, \dots, T$  and position  $x = 0, 1, 2, \dots, N-1$

**Ensure:** Edge-state survival probability at  $x=0$

- 1: Initialize the array storing the position-probability:  $\text{prob} \leftarrow 0$ s of the shape  $T+1 \times N$
- 2: Prepare initial state:

$$|\psi(0)\rangle = |0\rangle \otimes |c\rangle$$

where  $|c\rangle$  is a chosen internal coin state.

- 3: Define the SCSS-CQW single-step evolution operator (Eq. (6)):

$$\hat{U}_{evo} = \hat{S}_+ \hat{C}_\gamma \hat{S}_- \hat{C}_\gamma$$

- 4: **for** time step  $n = 1$  to  $n = T$ , **do**
- 5:     Update the quantum state of the quantum walker

$$|\psi(n)\rangle = \hat{U}_{evo}[|\psi(n-1)\rangle]$$

- 6:     **for** the position site 0 up to site  $(N-1)$ , **do**
- 7:         Evaluate site specific probability value (i.e.,  $P(x, n)$ ):

$$\sum_{g=0}^1 [(\langle x, g_c | \psi(n) \rangle) * (\langle x, g_c | \psi(n) \rangle)]$$

- 8:         Save the probability:  $\text{prob}[t][x]$  from the computed probability,  $[P(x, n)]$

- 9:     **end for.**

- 10: **end for.**

- 11: Compute edge-state survival probability:

$$P(x=0) = \text{prob}[t][0]$$

A pronounced value of  $P(x=0)$  serves as a hallmark of the generated edge state.

- 12: **return pro:** full spatio-temporal probability distribution of the SCSS-CQW.

The survival probability of the edge state at each time step is obtained as  $P(x=0)$  from the stored distribution, also see Python code [55]. This is used to analyze localization and robustness of the generated edge state via the SCSS-CQW protocol.